Transverse Peierls Transition

Kaifa Luo[1,2,4] and Xi Dai[3,4,*]

[1]Department of Physics, University of Texas at Austin, Austin, Texas 78712, USA
[2]Oden Institute for Computational Engineering and Sciences, University of Texas at Austin, Austin, Texas 78712, USA
[3]Materials Department, University of California, Santa Barbara, California 93106, USA
[4]Department of Physics, Hong Kong University of Science and Technology, Clear Water Bay, Hong Kong

(Received 20 April 2022; revised 13 October 2022; accepted 23 January 2023; published 28 February 2023)

We propose a new type of spontaneous symmetry breaking phase caused by softening of the transverse acoustic phonon modes through electron-phonon coupling. These new phases include the shear density wave and self-twisting wave, which are caused by softening of linearly and circularly polarized acoustic phonon modes, respectively. We propose that two of the topological semimetal systems in the quantum limit, where the electrons only occupy the lowest Landau bands under external magnetic field, will be the perfect systems to realize these new phases. Exotic physical effects will be induced in these new phases, including the 3D quantum Hall effect, chiral standing acoustic wave, magnetoacoustic effects, and chiral phonon correction to the Einstein–de Hass effect.

DOI: 10.1103/PhysRevX.13.011027

Subject Areas: Condensed Matter Physics, Materials Science

I. INTRODUCTION

The Peierls transition, which leads to charge density wave (CDW) [1,2] is one of the key phenomena caused by electron-phonon coupling [3,4] in condensed matter. It is induced by the so-called "nesting" feature of electron Fermi surfaces (FS), where two sections of the FS are connected by a single wave vector Q. The longitudinal acoustic (LA) phonon mode with wave vector Q is strongly coupled to electron-hole excitation between different sections of the FS by electron-phonon coupling, which leads to singular response at the low temperature and causes "condensation" of that particular phonon mode. The Peierls transition to CDW usually happens in 1D materials like polyacetylene, where energy bands disperse along the chain direction and a LA phonon with $Q = 2k_F$ connecting two Fermi points condenses at low temperature. Another very different system that shares a similar Peierls picture is a 3D semimetal material [5] under a strong magnetic field, where the electronic states are fully quantized to be Landau levels within the perpendicular plane and only disperse along the field direction. In the quantum limit, the Fermi level only crosses a single Landau band, which also satisfies the perfect nesting condition and leads to CDW. Comparing to 1D or quasi-1D materials, here the physics leading to completely flat band behavior along the perpendicular directions is not the lack of overlap between the neighboring electron wave functions but the Landau quantization. As a consequence, such a system has intrinsic 3D quantum Hall effect (QHE) [6,7] after CDW transition, which is quite different from the simple stacking of 2D quantum Hall layers [8], because the Landau level spacing is overwhelmed by band dispersion in the former cases and 3D QHE only appears after an energy gap is open by interactions. Such a theoretical proposal of potential 3D QHE associated with CDW has been suggested for over three decades before it was finally observed in Dirac material $ZrTe_5$ [9,10].

Comparing to QHE in 2D, much fruitful new physics will emerge in its 3D version. The most obvious difference is that 3D QHE is a spontaneous symmetry breaking phase under a strong magnetic field, which leads to new collective dynamics originated from dynamics of the order parameters. For incommensurate CDW, which is the case in 3D QHE with generic field strength, such collective modes are the "phason" modes along the field direction. How the sliding motion of CDW induced by the phason modes couples with the quantum Hall physics will be an interesting problem to explore.

The CDW and Peierls transition discussed so far in the 1D metal and 3D Landau band systems are both caused by the condensation of LA phonon modes. What about the transverse acoustic (TA) phonon mode? Can TA phonon modes also couple to electrons and condense? What kind of

*daix@ust.hk

new phases will be generated after condensation of TA phonon modes? These are key questions to be answered in the present paper. The results from our study reveal a completely different type of density wave instability associated with condensation of the TA phonon mode. Similar to the electromagnetic wave, a TA wave is also a type of vector wave, which can carry angular momentum. Along some high-symmetry directions, conservation of total angular momentum $j_z\hbar$ will lead to "selection rules" in the electron-TA phonon coupling, which is the analog of optical selection rules. Interestingly, depending on the detailed features of the low-energy electronic structure, the density waves caused by condensation of the TA phonons can be either linearly, elliptically, or circularly polarized, which are also similar to the light. The corresponding linearly polarized density wave is a unique type of shear strain with periodical modulation, and the circularly polarized density wave can be viewed as self-twisting of the crystal along the external field direction.

As we introduce in detail below, in the present work we have found two types of topological semimetals (TSMs) to realize the linearly and circularly polarized TA phonon condensation under magnetic field, respectively. One class is a Dirac semimetal with Dirac points being located along the high-symmetry axis. Because of the existence of inversion symmetry, the stable density wave in this case is the "shear strain wave" caused by linearly polarized TA phonon condensation. The chiral TA phonon condensation may happen in another noncentrosymmetric system, Kramers-Weyl semimetal, which is found to be a perfect type of material to form a "self-twisting wave" with the appearance of 3D QHE as its by-product.

II. MODEL

Let us start with a generic model describing a semimetal system with electron-phonon coupling,

$$\hat{H} = \frac{1}{N}\sum_{\alpha\beta\boldsymbol{k}} \mathcal{H}_{\alpha\beta\boldsymbol{k}} \hat{c}^{\dagger}_{\alpha\boldsymbol{k}} \hat{c}_{\beta\boldsymbol{k}} + \frac{1}{N}\sum_{\lambda\boldsymbol{q}} \hbar\omega_{\lambda\boldsymbol{q}} \hat{b}^{\dagger}_{\lambda\boldsymbol{q}} \hat{b}_{\lambda\boldsymbol{q}} + \frac{1}{N^{3/2}}\sum_{\substack{\alpha\beta\boldsymbol{k}\\ \lambda\boldsymbol{q}}} \mathcal{G}_{\alpha\beta\lambda\boldsymbol{k}\boldsymbol{q}} \hat{c}^{\dagger}_{\alpha\boldsymbol{k}+\boldsymbol{q}} \hat{c}_{\beta\boldsymbol{k}} (\hat{b}_{\lambda\boldsymbol{q}} + \hat{b}^{\dagger}_{\lambda,-\boldsymbol{q}}) + \text{H.c.}, \quad (1)$$

where $\mathcal{H}_{\alpha\beta\boldsymbol{k}}$ is electron $k\cdot p$ Hamiltonian with $\alpha(\beta)$ being band index, $\omega_{\lambda\boldsymbol{q}} = v^{\text{ph}}_{\lambda}|\boldsymbol{q}|$ is the acoustic phonon frequency with polarization $\lambda = x, y, z$ and speeds v^{ph}_{λ}, and $\mathcal{G}_{\alpha\beta\lambda\boldsymbol{k}\boldsymbol{q}}$ is the electron-phonon coupling matrix. $\hat{c}_{\alpha\boldsymbol{k}}$ and $\hat{b}_{\lambda\boldsymbol{q}}$ are annihilation operators of electron and phonon, respectively. N denotes the total number of unit cells. The system here has a discrete rotational symmetry $\hat{C}_{nz}$, and a strong external magnetic field $B_z\hat{\boldsymbol{z}}$ is applied. With respect to $\hat{C}_{nz}$, we adopt symmetric gauge $\boldsymbol{A} = (-y, x, 0)B_z/2$ in cylindrical geometry and apply the Peierls substitutions $k_{\pm} \to (-i\partial_x + eA_x/\hbar c) \pm i(-i\partial_y + eA_y/\hbar c)$ then. Under the magnetic field, in-plane motions of 3D electrons are fully quantized to form Landau levels and these "Landau bands" only disperse along z direction. In the long wavelength limit, discrete rotation symmetry in crystals can be approximated to be continuous and the total angular momentum $j_z\hbar$ is conserved, which contains orbital part $l^e_z\hbar = (m-n)\hbar$ [11] carried by the Landau level wave functions $|n, m\rangle$ (n is Landau level index and m the subindex) and internal part $s_z\hbar$ (which is called "spin" here) inherited from the $k\cdot p$ model. Thus, all electronic states are uniquely labeled as $\hat{c}^{\dagger}_{nmk_z}$ hereafter. Note that the effect of the direct coupling between charged ions and magnetic field is weak enough to be ignored (see Appendix A).

Assuming that both the rotation and translation symmetries are along the z axis, on a linearly polarized basis, the canonical coordinates of the TA phonon modes can be expressed as $\hat{X}_{\pm q_z} = (\hat{X}_{xq_z} \pm i\hat{X}_{yq_z})/\sqrt{2}$, which carry the orbital angular momenta $\pm\hbar$. In the cases of TSMs with both electron-phonon coupling and strong spin-orbit coupling (SOC), spin s_z, electron orbital l^e_z, and phonon orbital l^{ph}_z angular momenta are all coupled. However, n index is fixed in the quantum limit, and m is conserved. Thus, in our system, only s_z and l^{ph}_z are coupled (see Appendix B). As a result, three selection rules are enforced to electron-phonon coupling due to translation $\hat{T}_z$ and rotation $\hat{C}_z$ symmetries:

$$s_z = s'_z + l^{\text{ph}}_{z,\lambda}, \qquad m = m', \qquad k_z = k'_z + q_z. \quad (2)$$

It is worth noting that, different from the real transition process, here we focus on the virtual process caused by electron-phonon coupling where the conservation of energy is unnecessary.

When $q, k \ll l_B^{-1}$, the forms of electron-phonon coupling for both LA and TA phonon modes can be derived in a unified way using the Bir-Pikus formalism [12], which describes the strain potential with both hydrostatic and shear deformation effects included [13,14]. To be specific, a minimum nontrivial model with only two Landau bands is considered. Since these two bands (labeled by α, β) of our interest will hold the same n index, we drop it hereafter to lighten the notation. For a certain nesting wave vector Q, on a basis $\hat{\Psi}^{\dagger}_{mk_zQ} = (\hat{c}^{\dagger}_{s^{\alpha}_z mk_z+Q/2}, \hat{c}^{\dagger}_{s^{\beta}_z mk_z+Q/2}, \hat{c}^{\dagger}_{s^{\alpha}_z mk_z-Q/2}, \hat{c}^{\dagger}_{s^{\beta}_z mk_z-Q/2})^T$, with only $\hat{C}_z$ imposed, the specific form of electron-phonon coupling $\mathcal{G}_{mk_z\lambda Q}$, up to the zeroth order of k and the first order of q (see Appendix C 2) is

$$\begin{aligned} \mathcal{G}_{mk_z\pm,Q} &= iQ\xi_{\pm,Q} g_{\pm}\sigma_{\mp}\delta(s^{\alpha}_z - s^{\beta}_z - l^{\text{ph}}_{z,\pm}), \\ \mathcal{G}_{mk_zz,Q} &= iQ\xi_{zQ}(g_0\sigma_0 + g_z\sigma_z)\delta(s^{\alpha}_z - s^{\beta}_z), \end{aligned} \quad (3)$$

where Pauli matrices σ_{λ} span the pseudo-spin space and $\sigma_{\pm} = (\sigma_x \pm i\sigma_y)/2$, $\xi_{\lambda q_z} = \sqrt{\hbar/2M\omega_{\lambda q_z}}$ is the zero-point

displacement amplitude with M being the mass of ions in each unit cell, and g_λ are the coupling strength between electrons and phonons. For simplicity, here we set $g_0 = 0$.

Because of the nesting feature of the FS, the ionic motion will couple very strongly to the electronic degrees of freedom. Such a system is unstable and can be dealt with by the mean-field approach to replace the canonical coordinate operators with their expectation values $\langle \hat{X}_{\lambda Q} \rangle$, then the mean-field Hamiltonian per unit cell reads (see Appendix D 3)

$$\hat{\bar{H}}_Q = \frac{1}{N}\sum_{mk_z}(\mathcal{H}_{mk_zQ} + \Delta_{mk_zQ})\hat{\Psi}^\dagger_{mk_zQ}\hat{\Psi}_{mk_zQ} + \frac{M}{N}\sum_\lambda (g_\lambda^{-1} v_\lambda^{\mathrm{ph}} |\Delta_{\lambda Q}|)^2, \tag{4}$$

where $\mathcal{H}_{mk_zQ}$ now becomes the effective Hamiltonian on the basis $\hat{\Psi}^\dagger_{mk_zQ}$ in the reduced Brillouin zone $k_z \in [-Q/2, Q/2]$. The ratio of shear to longitudinal wave speeds is determined by Poisson's ratio σ through relation $v_T^{\mathrm{ph}}/v_z^{\mathrm{ph}} = \sqrt{(1-2\sigma)/(2-2\sigma)}$. The order parameter is a matrix, $\Delta_{mk_zQ} = \sum_\lambda \tau_+ \mathcal{G}_{mk_z\lambda Q}\Delta_{\lambda Q}/(iQ\xi_{\lambda Q}g_\lambda) + \mathrm{H.c.}$, and will be determined through self-consistent loop iteratively, where $\tau_\pm = (\tau_x \pm i\tau_y)/2$ span the valley degrees of freedom. In the following, we discuss two classes of realistic materials, Dirac and Kramers-Weyl semimetals.

III. REALISTIC MATERIALS

The first class of materials considered in the present study is Dirac semimetal, such as Na_3Bi [15–18], in which a pair of Dirac points located at k_z axis are protected by time reversal symmetry (TRS) $\hat{\mathcal{T}}$, inversion symmetry $\hat{\mathcal{P}}$, and rotation symmetry $\hat{\mathcal{C}}_{nz}$ ($n = 3$ for Na_3Bi), as shown in Fig. 1(a). Near Γ point, the effective Hamiltonian reads $\mathcal{H}^D_{\boldsymbol{k}} = (m_z k_z^2 + m_\perp k_+ k_- - m_0)\tau_z\sigma_0 + \hbar v_\perp(\tau_x\sigma_z - \tau_y\sigma_0) - \mu$ on basis $\hat{\Psi}^{D\dagger}_{\boldsymbol{k}} = (\hat{c}^\dagger_{1/2\boldsymbol{k}}, \hat{c}^\dagger_{-1/2\boldsymbol{k}}, \hat{c}^\dagger_{3/2\boldsymbol{k}}, \hat{c}^\dagger_{-3/2\boldsymbol{k}})^T$, where electron states are denoted as $\hat{c}^\dagger_{s_z\boldsymbol{k}}$. After the magnetic field is applied, the low-energy physics is dominated by two zeroth Landau bands with spin $s_z = 1/2$ and $-3/2$ as shown in Fig. 1(b). The basis becomes $\hat{c}_{s_z mk_z}$, and the effective magnetic Hamiltonian is $\mathcal{H}^D_{k_z} = (m_z k_z^2 - m_0)\sigma_z - \mu$ (see Appendix D 1). The FS contains four points (except $\mu = 0$), corresponding to states $\hat{c}^\dagger_{s_z,\pm k_{F,s_z}}$. Three phonons with different wave vectors are possible to participate in FS nesting, two intervalley $Q^D_{s_z}$ and one intravalley Q^D_T.

Enforced by the selection rules Eq. (2), the LA phonon mode is only allowed to participate in two intervalley scattering processes (connecting two electronic states with the same s_z) to form a CDW phase. Note that two different s_z states connected by the intervalley scattering are either both electron type or both hole type and will not contribute to the electron-hole-type instability. In contrast, the intravalley scattering process involving electronic states with different s_z can happen only when circularly polarized TA phonon modes ($l_z^{\mathrm{ph}} \neq 0$) are considered. Depending on the electron-phonon coupling strength g_λ, the competition between LA and TA phonons results in different phases, which are described by the Hamiltonian Eq. (4). The condensation of the LA phonon mode leads to ordinary CDW order, which spontaneously breaks the translation symmetry only. The situation of the TA phonon is quite different. Similar to electromagnetic wave, a TA phonon mode $\hat{X}_{\lambda q_z}$ has two polarizations, which can be expressed on circularly polarized basis $\hat{X}_{\pm,q_z} = (\hat{X}_{x,q_z} \pm i\hat{X}_{y,q_z})/\sqrt{2}$. When a TA phonon mode connects two different FS sections of the zeroth Landau bands as illustrated in Fig. 1(b), it can also be softened or even condensed. After condensation, in the generic case the expectation value of the phonon operators with both polarizations will be nonzero. Interestingly, the condensation of the TA phonon modes can be either linearly, elliptically, or circularly polarized depending on the relative phase factor $e^{i\phi_{xy}} = \langle \hat{X}_y \rangle / \langle \hat{X}_x \rangle$ between the order parameters of two orthogonal linearly polarized TA modes as summarized in Table I.

In particular, the presence of inversion symmetry in a Dirac semimetal will guarantee left- and right-handed

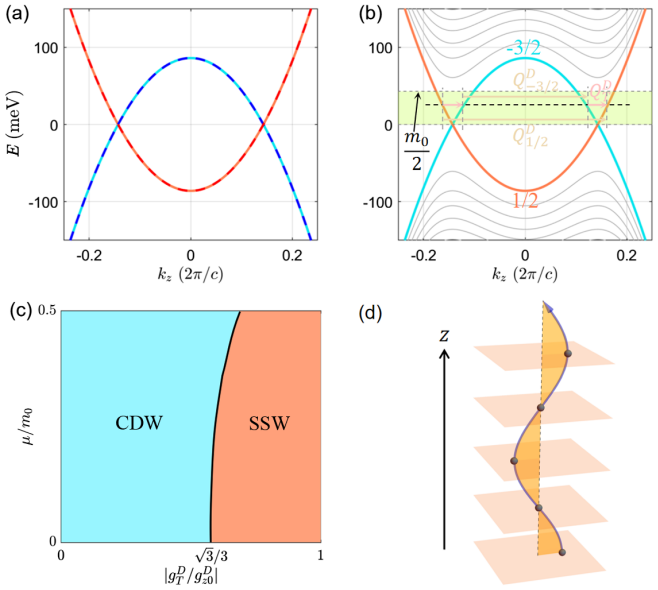

FIG. 1. Dirac semimetal. (a) Band structure near Γ point in k_z axis. (b) Zeroth Landau bands when $B_z = 10$ T. The area in olive drab denotes the regime of tunable chemical potential μ. (c) The ground state is either CDW with LA phonon softened (regime in blue) or shear strain wave with linearly polarized TA phonon softened (regime in burnt orange). When $\mu = 0$, effective coupling strength $|g^D_T/g^D_z| = v^{\mathrm{ph}}_T/v^{\mathrm{ph}}_z = \sqrt{3}/3$ is the phase boundary while it shifts to the right when μ increases. (d) Schematics of charge center (black dots) distribution in shear strain wave (SSW) phase.

TABLE I. Three types of polarizations of ground states caused by TA phonon condensation. Below n is an integer.

Relative phase	$\phi_{xy} = n\pi$	$\phi_{xy} \neq n\pi/2$	$\phi_{xy} = (2n+1)\pi/2$
Polarization	Linear	Elliptical	Circular

TA modes to be condensed with the same amplitudes, corresponding to a linearly polarized TA mode actually. Unlike charge redistribution along the wave vector in LA phonon condensation, the condensation of linearly polarized TA phonon generates a shear strain with periodicity Q_T^D instead, which is called a shear strain wave in our work. Based on the model parameters listed in Table II, the mean-field phase diagram is plotted in Fig. 1(c), in which CDW and shear strain wave phases are both possible to be stabilized in different regions of the parameter space. The key parameter determining the ground state is the ratio of coupling strength $|g_T^D/g_{z0}^D|$, which is the horizontal axis of Fig. 1(c). When it exceeds $v_T^{\mathrm{ph},D}/v_z^{\mathrm{ph},D} = \sqrt{3}/3$ at $\mu = 0$, the shear strain wave phase is more stable than the CDW phase. Note that, after the CDW or self-twisting wave phases have been stabilized, the Dirac semimetal becomes a trivial insulator rather than 3D QHE state because the energy gap is opened on the zeroth Landau bands.

Another class is Kramers-Weyl semimetal such as β-Ag_2Se [19,22,23], which is not centrosymmetric and circularly polarized TA phonons will not be suppressed by $\hat{\mathcal{P}}$. Unlike ordinary Weyl semimetals, the Weyl points in Kramers-Weyl semimetal are all pinned at the time reversal invariant momenta. For example, the band structure around Γ point is shown in Fig. 2(a). Assuming that the system contains a C_{nz} ($n = 2$ in β-Ag_2Se) symmetry, its $k \cdot p$ model near Γ point reads $\mathcal{H}_{\boldsymbol{k}}^{\mathrm{KW}} = (u_z k_z + u_\perp \boldsymbol{k}_\perp^2)\sigma_0 + (v_z k_z \sigma_z + v_\perp \boldsymbol{k}_\perp \cdot \boldsymbol{\sigma}_\perp) - \mu$ on basis $\hat{\Psi}_{\boldsymbol{k}}^{\mathrm{KW}\dagger} = (\hat{c}_{1/2\boldsymbol{k}}^\dagger, \hat{c}_{-1/2\boldsymbol{k}}^\dagger)^T$. Then in the quantum limit, the low-energy physics is dominated by two Landau bands with Landau band index $n = 1$ and spin $s_z = \pm 1/2$, as shown in Fig. 2(b) (see also Appendix D 2).

TABLE II. Model parameters for Dirac (Na_3Bi) [16] and Kramers-Weyl (β-Ag_2Se) [19] semimetals. The relative atomic mass $M_0 = 1.661 \times 10^{-27}$ kg and Landé g factor is set as 2. The superscript D (KW) in the symbols stands for Dirac (Kramers-Weyl) semimetals, while the subscript F stands for Fermi.

m_0	m_z	$m_\perp$	$\hbar v_\perp$	v_F^D
0.087 eV	10.64 eV Å^2	10.36 eV Å^2	2.46 eV Å	289 km/s
M^D/M_0	g_{z0}^D [20]	$v_z^{\mathrm{ph},D}$	σ^D	
556	0.5 eV	2650 m/s	0.25	
u_z	$u_\perp$	v_z	$v_\perp$	v_F^{KW}
−6 eV Å^2	$2.5u_z$	0.2 eV Å	$0.3v_z$	$v_z/\hbar$
M^{KW}/M_0	g_{z0}^{KW} [21]	$v_z^{\mathrm{ph,KW}}$	σ^{KW}	
1180	0.1 eV	2088 m/s	0.4	

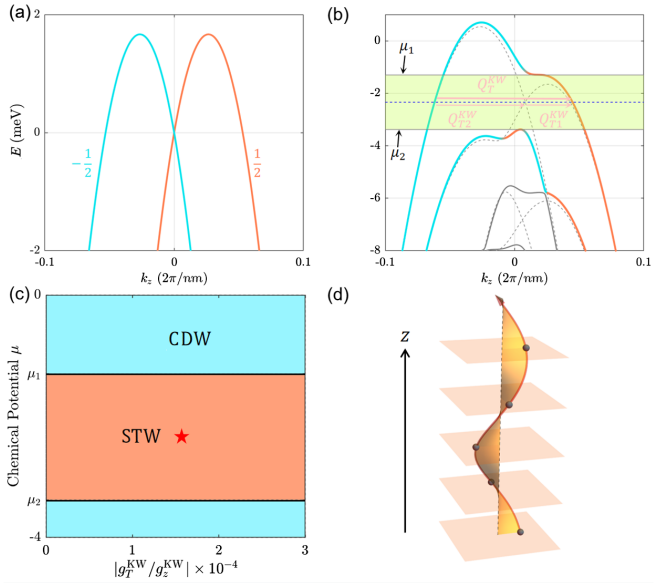

FIG. 2. Kramers-Weyl semimetals. (a) Band structure near Γ point in k_z axis. (b) Lowest Landau bands when magnetic fields $B_z = 10$ T and rotation symmetry breaking term δ_T are both applied, where the latter leads to a gap $2\delta_T = \mu_1 - \mu_2 = 2.4$ meV between $n = 1$ and 2 Landau bands. The color shades in red and blue denote proportions of wave functions with $s_z = \pm 1/2$, and they are mixed due to C_{2z} breaking. (c) The phase diagram of ground state has two regimes, where the area in burnt orange is self-twisting wave (STW) when Fermi level lies within the gap [area in olive of (b)] while other blue regimes are CDW phase. The red star marks the parameters used in Fig. 3. Here we set coupling constants $g_+ = 0.5g_-$. (d) Schematics of charge center (black dots) distribution in self-twisting wave phase.

To reach the nesting condition that the FS contains only two points, the Fermi level has to be placed inside the gap at the Γ point, which is generated by a rotational symmetry breaking term in addition to the magnetic field. Such a rotation symmetry breaking term can be generated by either the Zeeman effect of an additional in-plane magnetic field or some kinds of strain. Strictly speaking, the wave functions of different Landau bands are mixed by the symmetry breaking term and angular momentum is no long a good quantum number. However, such mixing of states with different angular momenta is only significant near the Γ point, while for states at the FS, the mixing effect is negligible and the angular momentum is still approximately conserved as well as the corresponding selection rule of electron-phonon coupling. Thus, in such a system the dominant instability happens for the circularly polarized TA phonons because of the selection rule. As a result, electron-phonon coupling will lead to self-twisting wave phase followed by the condensation of chiral TA phonon modes, as shown in Fig. 3(c). Since now the gap opens for the Landau bands with index $n = 1$, the electronic ground

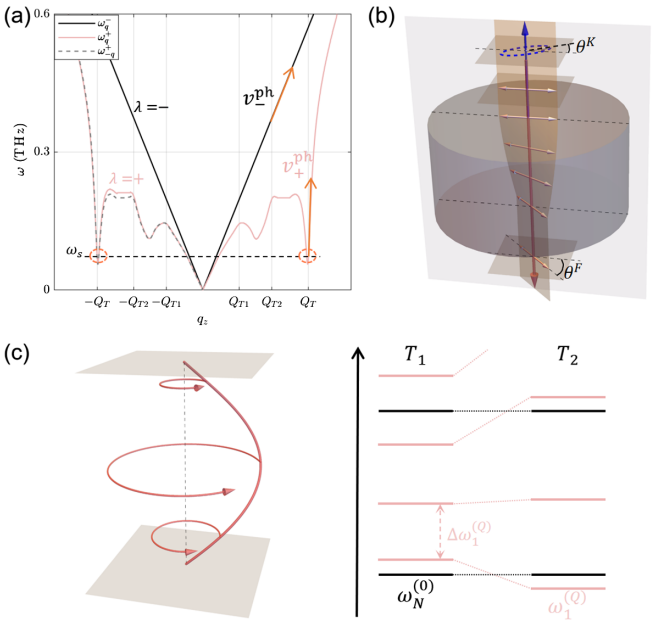

FIG. 3. Kramers-Weyl semimetals. (a) Renormalized TA phonon frequencies at $T = 1.1$ K (near $T_c \approx 1$ K). Here $|g_T/g_{z0}| = 1.43 \times 10^{-4}$ and the group speeds of left-handed (pink) and right-handed (black) chiral TA phonons are $v_\pm^{\rm ph}$. ω_s is the frequency of standing acoustic waves. (b) Magnetoacoustic effects. The gyromagnetic acoustic medium (cylinder in gray) is surrounded by regular medium. When a linearly polarized (two-headed arrow denotes the polarization direction) TA wave (red arrow) travels to the interface normally, the reflected wave (blue) becomes elliptical with Kerr ellipticity ϵ^K and rotation angle θ^K, while the polarization plane of refracted wave (red) gradually rotates by Faraday angle θ^F when it moves forward. (c) Left: schematics of left-handed chiral standing acoustic wave between two nodes. The red line denotes the amplitude of each center of mass and the arrows refer to its anticlockwise rotating trajectory. Right: resonant frequencies of standing modes. Given a finite length system at $T_1 = 1.1$ K, the frequencies of chiral standing modes with wave vector near Q_T are $\omega_{Q_T} + \Delta\omega_n^{(Q_T)}$, and of normal long wavelength standing modes (black) are $\omega_{n'}^{(0)}$. $\omega_N^{(0)}$ is the Nth normal standing mode close to $\omega_1^{(Q_T)}$. When the system is cooled down from T_1 to T_2 (~0.02 K), the frequencies of $\omega_n^{(0)}$ are almost the same, while the fundamental chiral mode ω_{Q_T} decreases rapidly and the frequency differences $\Delta\omega_n^{(Q_T)}$ increase.

state will have 3D QHE with quantized transverse conductance $\sigma_{\rm 3D} = Q_T^{\rm KW} e^2/h$.

IV. PHYSICAL EFFECTS

In this section, we discuss the possible exotic physical phenomena caused by the condensation or softening of the TA phonon modes. The first is the Goldstone mode in self-twisting wave phase. Similar to CDW phase where the sliding mode is a supercurrent of charge as a result of spontaneous breaking of translation symmetry, the chiral sliding mode in the incommensurate self-twisting wave phase is a supercurrent of angular momentum instead. Also, the new ground state will be a perfect chiral crystal, where the chiral phonon is discussed in recent works in the context of chiral [24], nonsymmorphic [25], and two-dimensional [26] materials.

More interesting effects are from acoustical activity [27–29]. To analyze frequency renormalization, the leading order of phonon self-energy is considered (Appendix E),

$$\Delta\omega_{\lambda q_z}^2 = (\omega_{\lambda q_z}^{\rm ren})^2 - \omega_{\lambda q_z}^2 = \frac{(g_T q_z)^2}{M}\mathcal{L}_{\lambda q_z}(\omega_{\lambda q_z}^{\rm ren}),$$
$$\mathcal{L}_{\lambda q_z} = \frac{1}{N}\sum_{\alpha\beta m k_z} \frac{(f_{\alpha k_z+q_z} - f_{\beta k_z})\delta(s_z^\alpha - s_z^\beta - l_{z,\lambda}^{\rm ph})}{\varepsilon_{\alpha k_z+q_z} - \varepsilon_{\beta k_z} - \hbar(\omega + i\eta)}, \quad (5)$$

where $\mathcal{L}_{\lambda q_z}$ is the Lindhard response function with $f_{\alpha k_z} \equiv f(\varepsilon_{\alpha k_z})$ being Fermi-Dirac distribution. At low temperature $T < \delta_T/k_B$, where the gap will not be smeared out by thermal fluctuation, the TA phonon frequencies at long wavelength regime are almost unscreened and quasi-degenerate, while two different branches of chiral phonons deviate hugely near wave vector Q_T. The effective dispersion of the left-handed phonon branch near $\pm Q_T$ is $\omega_{\delta q_z}^{(\pm Q_T)} = \omega_{Q_T} + b(\delta q_z)^2/2$ with $\omega_{Q_T} \propto \sqrt{(T - T_c)/T_c}$ [2] before phase transition happens (T higher than critical temperature T_c), and $b = 8.71 \times 10^{-4}$ m^2/s is fitted at $T = 1.1$ K. Thus, the system is a gyromagnetic medium with acoustical activity, in which the group speed of the right-handed phonon branch is still $v_T^{\rm ph}$, and that of the left-handed chiral waves is renormalized to $v_{\delta q_z}^{(\pm Q_T)} = \partial\omega_{\delta q_z}^{(\pm Q_T)}/\partial(\delta q_z) = b\delta q_z$, as shown in Fig. 3(a).

After the degeneracy of TA phonon modes is lifted by electron-phonon coupling, a series of magnetoacoustic effects immediately follow, such as Faraday, Kerr, Cotton-Mouton, or Voigt effects [29,30]. As examples, here we discuss Faraday rotation and Kerr ellipticity as results of magnetoacoustic circular birefringence, which are also found in α quartz [31,32] and superfluid ^{3}He-B [33,34]. Consider a setup in which the gyromagnetic acoustic medium is surrounded by a normal medium such as chlorinated polyvinyl chloride (CPVC) with shear acoustic wave speed 1060 m/s. In the polar configuration, if a linearly polarized TA wave with frequency $\omega > \omega_{Q_T}$ travels from the CPVC side to the gyromagnetic medium, the reflected wave from the interface will become elliptical, while the polarization plane of refracted wave in the gyromagnetic medium will gradually rotate, as shown in Fig. 3(b). Under external magnetic induction $B_z = 10$ T at $T = 1.1$ K, for acoustic wave with frequency $\omega = 58.0$ GHz, a significant Kerr ellipticity $\epsilon^K = 0.41$, and a giant Faraday angle per distance 1.77×10^5 rad/cm (see Appendix G) are estimated to be measured. Other typical effects, such as Faraday ellipticity

and Kerr rotation induced by magnetoacoustic circular dichroism, can also be observed.

Another easily observed signature of magnetoacoustic circular refringence is resonant frequency of chiral standing acoustic wave, as shown in Fig. 3(c). Given a system at $T_1 = 1.1$ K with length $d = 1$ cm along the z axis, the resonant frequencies of the left-handed chiral modes with wave vector around Q_T are $\omega_{Q_T} + \Delta\omega_n^{(Q_T)} = 56.1$ GHz + $0.086(n + 1/2)$ kHz and of the normal long wavelength standing modes are $\omega_n^{(0)} = (268n)$ kHz (see Appendix F). Because the electronic screening leads to the frequency local minimum $\omega_{Q_T} \propto \sqrt{(T - T_c)/T_c}$ [2], a tiny temperature change will lead to a significant lowering of fundamental mode frequency of the chiral standing waves as well as an increase of frequency differences. For example, ω_{Q_T} will decrease to 48.1 GHz and $\Delta\omega_n^{(Q_T)}$ increase to $0.097(n + 1/2)$ kHz if the system is cooled down to $T = 1.08$ K. Similar temperature sensitive behaviors of resonances can also be observed in shear strain wave phase of Dirac semimetal, while the standing modes are not chiral but linearly polarized.

In the end, we would also mention the chiral phonon correction to the Einstein–de Hass effect. When electron-phonon coupling is turned off and the direct coupling of ions to magnetic field is neglected, TRS will pair two phonons with opposite angular momenta as $\hat{\mathcal{T}}\hat{X}_{+,\boldsymbol{q}}\hat{\mathcal{T}}^{-1} = \hat{X}_{-,-\boldsymbol{q}}$, resulting in a zero net phonon angular momenta, which is one of the premises in the original proposal of the Einstein–de Hass effect [35]. However, the TRS of the TA phonon subsystem is broken mediated by the electron-phonon coupling. As a result, the nonzero net phonon angular momentum has to be included in the conservation law of total angular momentum and will lead to an observable correction to the Einstein-de Hass effect. This correction is also investigated in the work of Zhang and Niu [36] where they discussed spin-phonon coupling. For β-Ag_2Se under external magnetic field $B = 5$ T at temperature $T = 15.7$ K, the net phonon angular momentum per unit cell is estimated to be $1.5 \times 10^{-3}\hbar$ (see Appendix I).

V. CONCLUSION AND OUTLOOK

The interaction between electron and TA phonon mode has been overlooked for decades. In this article, we have proposed two kinds of exotic condensation of TA phonon modes, shear strain wave and self-density wave, induced by electron-TA phonon coupling in specific TSMs under magnetic field. We find that when a strong enough magnetic field is applied along the rotational axis of Dirac and Kramers-Weyl semimetal materials, the low-energy electronic states can be described by their zeroth or lowest Landau bands with different internal angular momentum $s_z\hbar$. The presence of rotational symmetry enforces important selection rules to electron-phonon coupling terms for both LA and TA phonons. The combination of FS nesting and the selection rules of electron-phonon coupling induce two exotic new density wave states. The linearly polarized TA phonon condensation leads to a shear strain wave state while circularly polarized TA phonon condensation gives us a self-twisting state. The self-twisting phase is a typical chiral matter, which can lead to a number of new physical effects including chiral sliding mode, chiral standing wave, magnetoacoustic effects, and chiral phonon correction to the Eistein–de Hass effect.

ACKNOWLEDGMENTS

The authors thank Qian Niu and Yafei Ren for valuable discussions. X. D. acknowledges financial support from the Hong Kong Research Grants Council (Projects No. GRF16300918 and No. 16309020). K. L. acknowledges the Texas Advanced Computing Center (TACC) at The University of Texas at Austin for providing HPC resources that have contributed to the first-principles calculation results reported within this paper.

APPENDIX A: CHARGED HARMONIC OSCILLATOR IN UNIFORM MAGNETIC FIELD

To estimate the magnitude of direct coupling of magnetic field on lattice (ions) vibration, here we consider a simplest 3D harmonic oscillator carrying Ze charges. By minimal coupling to vector potential $\boldsymbol{A}$, its Hamiltonian reads

$$\begin{aligned}\hat{H}^{\mathrm{ph}} &= \frac{1}{2M}[(\hat{P}_x - ZeA_x)^2 + (\hat{P}_y - ZeA_y)^2 + \hat{P}_z^2] + \frac{1}{2}M\omega_T^2(\hat{X}_x^2 + \hat{X}_y^2) + \frac{1}{2}M\omega_z^2\hat{X}_z^2 \\ &= \left\{\frac{1}{2M}(\hat{P}_x^2 + \hat{P}_y^2) + \frac{1}{2}M\left[\omega_T^2 + \left(\frac{ZeB}{2M}\right)^2\right](\hat{X}_x^2 + \hat{X}_y^2)\right\} + \left(\frac{1}{2M}\hat{P}_z^2 + \frac{1}{2}M\omega_z^2\hat{X}_z^2\right) - \frac{ZeB}{2M}\hat{L}_z \\ &= \left[\frac{1}{2M}(\hat{P}_x^2 + \hat{P}_y^2) + \frac{1}{2}M\tilde{\omega}_T^2(\hat{X}_x^2 + \hat{X}_y^2)\right] + \left(\frac{1}{2M}\hat{P}_z^2 + \frac{1}{2}M\omega_z^2\hat{X}_z^2\right) - \frac{Zm_e}{M\hbar}\mu_B B\hat{L}_z, \\ \tilde{\omega}_T^2 &= \omega_T^2 + \left(\frac{Zm_e}{M\hbar}\mu_B B\right)^2, \end{aligned} \tag{A1}$$

where M is the mass and ω_z and ω_T are eigenenergies in the z axis and xy plane (given rotation symmetry along the z axis). $\hat{L}_z = \hat{X}_x\hat{P}_y - \hat{P}_x\hat{X}_x$ is z component of orbital angular momentum operator. Comparing to the unperturbed Hamiltonian $\hat{H}^{\mathrm{ph}}(\boldsymbol{A} = \boldsymbol{0})$, two in-plane effects are introduced: the degenerate eigenfrequencies of states in xy plane shifting from ω_T to $\tilde{\omega}_T$, and the splitting $\Delta\omega_T = 2(Zm_e\mu_B B/M\hbar^2)\hat{L}_z$ between chiral modes with different orbital angular momenta. Now we can do a rough estimation: assuming that the frequency of a certain phonon mode in realistic materials is around $\omega_T = 1$ THz (speed $v_T^{\mathrm{ph}} = 2\times 10^3$ m/s and wave vector $q_z = 0.5\times 10^9$ m^{-1}, smaller than $1/10$ scale of the first BZ), the mass ratio of the electron to the ion $m_e/M \sim 10^{-6}$, the effective charge of ion $Z \sim 10$, and $\mu_B B/\hbar \approx 1$ THz when $B_z = 10$ T. Taking the unperturbed frequency ω_T as a reference, the order of magnitude of shifting and splitting are around $|\tilde{\omega}_T - \omega_T|/\omega_T \approx 10^{-10}$ and $\Delta\omega_T/\omega_T \approx 10^{-5}$ given $|L_z| = \hbar$. Therefore, it is sensible to ignore both of these effects and treat phonons as neutral particles when we investigate electron-phonon coupling.

APPENDIX B: SELECTION RULES IN SYMMETRIC GAUGE

In this appendix, we specify that, in the quantum limit, indices n and m are conserved separately and then derive the selection rules in electron-phonon coupling. Let us start with the orbital angular momentum of the spinless 2D electron gas. When a uniform magnetic field with symmetric gauge $\boldsymbol{A} = (-y, x, 0)B/2$ is applied, the Hamiltonian reads

$$\hat{H}^{\mathrm{2D}} = \frac{1}{2m}[(-i\hbar\partial_x - yeB/2)^2 + (-i\hbar\partial_y + xeB/2)^2] = \frac{1}{2m}(\hat{\pi}_x^2 + \hat{\pi}_y^2), \tag{B1}$$

where $\hat{\pi}_{x,y}$ are covariant momenta. Based on the guiding-center coordinates $\hat{r}_x = \hat{x} + \hat{\pi}_y/eB$ and $\hat{r}_y = \hat{y} - \hat{\pi}_x/eB$, we can define two annihilation operators,

$$\hat{a} = \frac{l_B}{\sqrt{2}\hbar}(\hat{\pi}_x + i\hat{\pi}_y), \qquad \hat{b} = \frac{l_B}{\sqrt{2}\hbar}(\hat{r}_x - i\hat{r}_y), \tag{B2}$$

with magnetic length $l_B = \sqrt{\hbar/eB}$ and commutation relations $[\hat{a}, \hat{a}^\dagger] = [\hat{b}, \hat{b}^\dagger] = 1$, $[\hat{a}, \hat{b}] = [\hat{a}^\dagger, \hat{b}] = 0$. Then all Landau wave functions are able to be constructed as $|n, m\rangle = (n!m!)^{-1/2}(\hat{a}^\dagger)^n(\hat{b}^\dagger)^m|0\rangle$, where n, m are Landau level index and subindex, respectively. Then the Hamiltonian can be rewritten as $\hat{H} = (\hat{a}^\dagger\hat{a} + 1/2)\hbar\omega_c$ (cyclotron frequency $\omega_c = eB/m$), which is only dependent on Landau level index and all Landau level states distinguished by different m quantum number are highly degenerate. The continuous rotation symmetry gives us a conserved quantity, canonical orbital angular momentum,

$$\hat{L}_z = -i\hbar(x\partial_y - y\partial_x) = \frac{B}{2}(\hat{r}_x^2 + \hat{r}_y^2) - \frac{1}{2eB}(\hat{\pi}_x^2 + \hat{\pi}_y^2) = (\hat{b}^\dagger\hat{b} - \hat{a}^\dagger\hat{a})\hbar \equiv \hat{L}_z^{(m)} + \hat{L}_z^{(n)}, \tag{B3}$$

where $\hat{L}_z^{(n)} = -\hat{a}^\dagger\hat{a}\hbar$, $\hat{L}_z^{(m)} = \hat{b}^\dagger\hat{b}\hbar$, and $[\hat{L}_z^{(n)}, \hat{L}_z^{(m)}] = 0$. Now we know a state $|n, m\rangle$ carries orbital angular momentum $L_z = (m - n)\hbar$.

For a generic continuum model of 3D spinful electron under magnetic field $B_z\hat{\boldsymbol{z}}$, the xy-plane orbital motions are still described on the basis of Landau wave functions $|n, m\rangle$, and only the total angular momentum $(s_z + m - n)\hbar$ is conserved. Since Hamiltonian $\mathcal{H}_{k_z}^{\alpha\beta}(-i\partial_x + eA_x/\hbar c, -i\partial_y + eA_y/\hbar c)$ is quantized to $\hat{\mathcal{H}}_{k_z}^{\alpha\beta}((\hat{a}^\dagger + \hat{a})/\sqrt{2}l_B, (\hat{a}^\dagger - \hat{a})/i\sqrt{2}l_B)$, all SOC terms are only related to $L_z^{(n)}$ and irrelevant to $L_z^{(m)}$. Therefore, the conservation of angular momenta is actually able to be separated into two parts:

$$s_z + n = s_z' + n', \qquad m = m'. \tag{B4}$$

As will be discussed in the next appendix, the electron-phonon coupling we obtained only involves the spin flip and it only happens within Landau bands with the same indices $n = n'$, so the selection rules arrive at a quite demanding form:

$$s_z = s_z' + l_{z,\lambda}^{\mathrm{ph}}, \qquad m = m', \tag{B5}$$

where $l_{z,\lambda}^{\mathrm{ph}}$ is the orbital angular momentum of a certain phonon with polarization λ.

APPENDIX C: ELECTRON-PHONON COUPLING

1. Bir-Pikus formalism

The lattice vibration in the continuum limit is a time-dependent local strain $\hat{\boldsymbol{\varepsilon}}(\boldsymbol{r}, t)$. For the small amplitude of ions' displacement $\hat{u}_\lambda(\boldsymbol{r}) = N^{-1/2}\sum_{\boldsymbol{q}}\hat{X}_{\lambda\boldsymbol{q}}e^{i\boldsymbol{q}\cdot\boldsymbol{r}}$ compared with the scale of the unit cell, the quantized strain operator in terms of phonon creation and annihilation operators is

$$\hat{\varepsilon}_{ij}(\boldsymbol{r}) = \frac{1}{\sqrt{N}}\sum_{\boldsymbol{q}} iq_j \hat{X}_{i\boldsymbol{q}} e^{i\boldsymbol{q}\cdot\boldsymbol{r}} = \frac{1}{\sqrt{N}}\sum_{\boldsymbol{q}} iq_j \xi_{i\boldsymbol{q}} (\hat{b}_{i\boldsymbol{q}} + \hat{b}^{\dagger}_{i,-\boldsymbol{q}}) e^{i\boldsymbol{q}\cdot\boldsymbol{r}}, \tag{C1}$$

with $\xi_{\lambda\boldsymbol{q}} = \sqrt{\hbar/2M\omega_{\lambda\boldsymbol{q}}}$, and it is natural to treat it by perturbation theory. However, a generic deformed lattice potential $V^{\varepsilon}(\boldsymbol{r})$ does not have the same periodicity as the original one $V^0(\boldsymbol{r})$ and the regular perturbation theory is not justified any more since the wave function of the perturbed Hamiltonian is always expressed as a superposition of wave functions of the unperturbed $\hat{H}^0$ satisfying the same boundary conditions. The same difficulty shows up when Bir and Pikus tried to tame the effect of a homogeneous strain [12]. Therefore, we develop their formalism to deal with the effect of lattice vibration and transform the coordinates to make the periodicity in the new coordinate system coincide with the unstrained situation in the old coordinate system. Up to linear order of strain, this is done by putting

$$r'_i = r_i + \hat{\varepsilon}_{ij} r_j, \qquad \hat{p}'_i = -i\hbar\frac{\partial}{\partial r'_i} = \hat{p}_i - \hat{\varepsilon}_{ij}\hat{p}_j, \tag{C2}$$

where $\boldsymbol{r}$, $\boldsymbol{p}$ are electron's coordinate and momentum, and the transformation between the reciprocal vectors is

$$k'_i = k_i - \hat{\varepsilon}_{ij} k_j. \tag{C3}$$

Correspondingly, the Bloch function in the deformed system becomes

$$e^{i\boldsymbol{k}'\cdot\boldsymbol{r}'} u_{n\boldsymbol{k}'}(\boldsymbol{r}') = e^{i\boldsymbol{k}\cdot\boldsymbol{r}} u_{n\boldsymbol{k}'}\big((1+\hat{\boldsymbol{\varepsilon}})\boldsymbol{r}\big) \equiv e^{i\boldsymbol{k}\cdot\boldsymbol{r}} u'_{n\boldsymbol{k}}(\boldsymbol{r}), \tag{C4}$$

having the same phase factor as in an undeformed system. By this way, we are safe to use perturbation theory and the difference of the Hamiltonian can be expanded in terms of $\hat{\varepsilon}_{ij}$,

$$\begin{aligned}\hat{H}^0 &= \frac{\hat{\boldsymbol{p}}^2}{2m_0} + V^0(\boldsymbol{r}) + \frac{\hbar}{4m_0^2c^2}(\hat{\boldsymbol{\sigma}}\times\nabla V^0)\cdot\hat{\boldsymbol{p}},\\ \hat{H}^{ep} &= \hat{H}^{\varepsilon}(\boldsymbol{r}',\hat{\boldsymbol{p}}') - \hat{H}^0(\boldsymbol{r},\hat{\boldsymbol{p}}),\end{aligned} \tag{C5}$$

so the strained electron Hamiltonian in the original coordinates transforms into the deformed coordinates:

$$\begin{aligned}\hat{H}^{\varepsilon}(\boldsymbol{r}',\hat{\boldsymbol{p}}') &= \frac{\hat{\boldsymbol{p}}'^2}{2m_0} + V^{\varepsilon}(\boldsymbol{r}') + \frac{\hbar}{4m_0^2c^2}[\hat{\boldsymbol{\sigma}}\times\nabla' V^{\varepsilon}(\boldsymbol{r}')]\cdot\hat{\boldsymbol{p}}'\\ &= \frac{[(1-\hat{\boldsymbol{\varepsilon}})\hat{\boldsymbol{p}}]^2}{2m_0} + V^{\varepsilon}\big((1+\hat{\boldsymbol{\varepsilon}})\boldsymbol{r}\big) + \frac{\hbar}{4m_0^2c^2}\{\hat{\boldsymbol{\sigma}}\times[(1-\hat{\boldsymbol{\varepsilon}})\nabla]V^{\varepsilon}\big((1+\hat{\boldsymbol{\varepsilon}})\boldsymbol{r}\big)\}\cdot(1-\hat{\boldsymbol{\varepsilon}})\hat{\boldsymbol{p}}\\ &= \hat{H}^0(\boldsymbol{r},\hat{\boldsymbol{p}}) - \frac{1}{m_0}\hat{p}_i\hat{\varepsilon}_{ij}\hat{p}_j + V_{ij}\hat{\varepsilon}_{ij} - \frac{\hbar}{4m_0^2c^2}\epsilon_{ijk}\hat{\sigma}_i[(\partial_j V^0)\hat{\varepsilon}_{kt}\hat{p}_t + (\hat{\varepsilon}_{jl}\partial_l V^0)\hat{p}_k - (\partial_j V_{lm}\hat{\varepsilon}_{lm})\hat{p}_k],\end{aligned} \tag{C6}$$

where $V_{ij} \equiv \lim_{\varepsilon\to 0}[V^{\varepsilon}\big((1+\hat{\varepsilon})\boldsymbol{r}\big) - V^0(\boldsymbol{r})]/\hat{\varepsilon}_{ij}$, and we used a commutation relation:

$$[\hat{p}_i,\hat{\varepsilon}_{jk}] = \frac{1}{\sqrt{N}}\sum_{\boldsymbol{q}} iq_k\xi_{j\boldsymbol{q}}(\hat{b}_{j\boldsymbol{q}} + \hat{b}^{\dagger}_{j,-\boldsymbol{q}})[\hat{p}_i, e^{i\boldsymbol{q}\cdot\boldsymbol{R}}] = \frac{1}{\sqrt{N}}\sum_{\boldsymbol{q}} iq_k\xi_{j\boldsymbol{q}}(\hat{b}_{j\boldsymbol{q}} + \hat{b}^{\dagger}_{j,-\boldsymbol{q}})(\hbar q_i e^{i\boldsymbol{q}\cdot\boldsymbol{R}}) = 0 + \mathcal{O}(q^2), \tag{C7}$$

then

$$\begin{aligned}[(1-\hat{\boldsymbol{\varepsilon}})\nabla]V^{\varepsilon}\big((1+\hat{\boldsymbol{\varepsilon}})\boldsymbol{r}\big) &= (\partial_i - \hat{\varepsilon}_{ij}\partial_j)(\hat{V}_0 + V_{lm}\hat{\varepsilon}_{lm})\hat{e}_i = (\partial_i V^0 - \hat{\varepsilon}_{ij}\partial_j V^0 + \partial_i V_{lm}\hat{\varepsilon}_{lm})\hat{e}_i,\\ \{\hat{\boldsymbol{\sigma}}\times[(1-\hat{\boldsymbol{\varepsilon}})\nabla]V^{\varepsilon}\big((1+\hat{\boldsymbol{\varepsilon}})\boldsymbol{r}\big)\}\cdot(1-\hat{\boldsymbol{\varepsilon}})\hat{\boldsymbol{p}} &= \epsilon_{ijk}\hat{\sigma}_i(\partial_j V^0 - \hat{\varepsilon}_{jl}\partial_l V_0 + \partial_j V_{lm}\hat{\varepsilon}_{lm})(\hat{p}_k - \hat{\varepsilon}_{kt}\hat{p}_t)\\ &= \epsilon_{ijk}\hat{\sigma}_i[(\partial_j V^0)\hat{p}_k - (\partial_j V^0)\hat{\varepsilon}_{kt}\hat{p}_t - (\hat{\varepsilon}_{jl}\partial_l V^0)\hat{p}_k + (\partial_j V_{lm}\hat{\varepsilon}_{lm})\hat{p}_k]\\ &= \hat{\boldsymbol{\sigma}}\times\nabla V^0\cdot\hat{\boldsymbol{p}} - \hat{\boldsymbol{\sigma}}\times\nabla V^0\cdot(\hat{\boldsymbol{\varepsilon}}\hat{\boldsymbol{p}}) - \hat{\boldsymbol{\sigma}}\times(\hat{\boldsymbol{\varepsilon}}\nabla V^0)\cdot\hat{\boldsymbol{p}} + \hat{\boldsymbol{\sigma}}\times\nabla(\hat{\boldsymbol{\varepsilon}}\boldsymbol{V})\cdot\hat{\boldsymbol{p}},\end{aligned} \tag{C8}$$

where we denote $\hat{\boldsymbol{\varepsilon}}\boldsymbol{V} \equiv \hat{\varepsilon}_{lm}V_{lm}$ following the original notation by Bir and Pikus. Then we have

$$\begin{aligned}\hat{H}^{ep} &= \boldsymbol{V}\hat{\boldsymbol{\varepsilon}} - \frac{1}{m_0}\hat{\boldsymbol{p}}\,\hat{\boldsymbol{\varepsilon}}\,\hat{\boldsymbol{p}} + \frac{\hbar}{4m_0^2c^2}[\hat{\boldsymbol{\sigma}}\times\nabla(\hat{\boldsymbol{\varepsilon}}\boldsymbol{V})\cdot\hat{\boldsymbol{p}} - \hat{\boldsymbol{\sigma}}\times\nabla V^0\cdot(\hat{\boldsymbol{\varepsilon}}\hat{\boldsymbol{p}}) - \hat{\boldsymbol{\sigma}}\times(\hat{\boldsymbol{\varepsilon}}\nabla V^0)\cdot\hat{\boldsymbol{p}}]\\ &= -\frac{1}{m_0}\hat{\pi}_i\hat{\varepsilon}_{ij}\hat{p}_j - \frac{\hbar}{4m_0^2c^2}(\hat{\boldsymbol{p}}\times\hat{\boldsymbol{\sigma}})_i\hat{\varepsilon}_{ij}\partial_j V^0 + V_{ij}\hat{\varepsilon}_{ij} + \frac{\hbar}{4m_0^2c^2}\hat{\boldsymbol{\sigma}}\times(\hat{\varepsilon}_{ij}\nabla V_{ij})\cdot\hat{\boldsymbol{p}}\\ &= \hat{\varepsilon}_{ij}\hat{\mathcal{V}}_{ij} + \mathcal{O}(q^2),\end{aligned} \tag{C9}$$

where $\hat{\boldsymbol{\pi}} = \hat{\boldsymbol{p}} + (\hat{\boldsymbol{\sigma}} \times \nabla \hat{V}_0)\hbar/4m_0c^2$, and note that $\hat{\boldsymbol{\sigma}} \times (\nabla \hat{\boldsymbol{\epsilon}})\boldsymbol{V} \cdot \hat{\boldsymbol{p}}$ is in the order of q^2. Here $\hat{\mathcal{V}}_{ij}$ is a rank-2 tensor operator. Then the Schrödinger equation becomes

$$(\hat{H}^0 + \hat{H}^{ep})e^{i\boldsymbol{k}\cdot\boldsymbol{r}}u'_{n\boldsymbol{k}}(\boldsymbol{r}) = E'_{n\boldsymbol{k}}e^{i\boldsymbol{k}\cdot\boldsymbol{r}}u'_{n\boldsymbol{k}}(\boldsymbol{r}) \Rightarrow \hat{H}^{\epsilon}(\boldsymbol{k})u'_{n\boldsymbol{k}}(\boldsymbol{r}) = E'_{n\boldsymbol{k}}u'_{n\boldsymbol{k}}(\boldsymbol{r}). \tag{C10}$$

In the end, we arrive at the strained $k \cdot p$ Hamiltonian,

$$\begin{aligned}
\hat{H}^{\epsilon}(\boldsymbol{k}) &= \hat{H}^0 + \hat{H}^0_{\boldsymbol{k}} + \hat{H}^{ep} + \hat{H}^{ep}_{\boldsymbol{k}}, \\
\hat{H}^0_{\boldsymbol{k}} &= \frac{\hbar^2 k^2}{2m_0} + \frac{\hbar}{m_0}\boldsymbol{k} \cdot \hat{\boldsymbol{\pi}}, \\
\hat{H}^{ep}_{\boldsymbol{k}} &= \frac{\hbar^2 \hat{\epsilon}_{ij}k_i k_j}{m_0} + \frac{\hbar}{m_0}(\hat{\epsilon}_{ij} + \hat{\epsilon}_{ji})k_i\hat{p}_j + \frac{\hbar^2}{4m_0^2c^2}[\hat{\boldsymbol{\sigma}} \times \nabla(\hat{\boldsymbol{\epsilon}}\boldsymbol{V}) \cdot \boldsymbol{k} - \hat{\boldsymbol{\sigma}} \times \nabla V^0 \cdot (\hat{\boldsymbol{\epsilon}}\boldsymbol{k}) - \hat{\boldsymbol{\sigma}} \times (\hat{\boldsymbol{\epsilon}}\nabla V^0) \cdot \boldsymbol{k}],
\end{aligned} \tag{C11}$$

where the first two terms of $\hat{H}^{ep}_{\boldsymbol{k}}$ are nonrelativistic effects and all others are the contributions from SOC. In this work, we only consider electron-phonon coupling up to the zeroth order of $\boldsymbol{k}$, so $\hat{H}^{ep}_{\boldsymbol{k}}$ is ignored in the following. Note that, if we are interested in Hamiltonian up to first order of $\boldsymbol{q}$, treating strain tensor $\boldsymbol{\epsilon}$ as a classical quantity during all the derivations then quantizing it at the very end in Eq. (C11) will obtain the same result. Because we focus on phonons with well-defined angular momenta along z direction, i.e., nonzero components are $\hat{\epsilon}_{iz}$ $(i = x, y, z)$, we only need to concern $\hat{\mathcal{V}}_{iz}$ terms and the others have no contributions to electron-phonon coupling. Keeping these nonzero coefficients in mind, the spherical components are defined as

$$\hat{\mathcal{V}}_0 = \hat{\mathcal{V}}_{zz}, \qquad \hat{\mathcal{V}}_{\pm 1} = \frac{1}{2}(\hat{\mathcal{V}}_{xz} \pm i\hat{\mathcal{V}}_{yz}), \qquad \hat{\mathcal{V}}_{\pm 2} = 0. \tag{C12}$$

As followed, we rewrite the electron-phonon coupling in terms of these symmetric components,

$$\hat{H}^{ep} = \hat{\epsilon}_{zz}\hat{\mathcal{V}}_{zz} + \hat{\epsilon}_{+,z}\hat{\mathcal{V}}_{-1} + \hat{\epsilon}_{-,z}\hat{\mathcal{V}}_{+1}, \tag{C13}$$

where $\hat{\epsilon}_{\pm,z} = \hat{\epsilon}_{x,z} \pm i\hat{\epsilon}_{y,z}$. Now we arrive at the matrix elements of electron-phonon coupling Hamiltonian on chiral phonon basis,

$$\begin{aligned}
\langle \psi_{s_z^\alpha mk_z}|\hat{\epsilon}_{\pm,z}\hat{\mathcal{V}}_{\mp 1}|\psi_{s_z^\beta m'k'_z}\rangle &= \frac{1}{\sqrt{N}} iq_z\xi_{\pm,q_z}(\hat{b}_{\pm,q_z} + \hat{b}^\dagger_{\pm,-q_z})\langle u_{s_z^\alpha mk_z}|e^{i(k'_z+q_z-k_z)z}\hat{\mathcal{V}}_{\mp 1}|u_{s_z^\beta m'k'_z}\rangle\delta(m'-m) \\
&= \frac{1}{\sqrt{N}} iq_z\xi_{\pm,q_z}(\hat{b}_{\pm,q_z} + \hat{b}^\dagger_{\pm,-q_z})\langle u_{s_z^\alpha mk_z+q_z}|\hat{\mathcal{V}}_{\mp 1}|u_{s_z^\beta mk_z}\rangle\delta(k'_z+q_z-k_z)\delta(s_z^\alpha - s_z^\beta - l^{\mathrm{ph}}_{z,\pm,q_z}) \\
&\equiv \frac{1}{\sqrt{N}}\mathcal{G}_{mk_z\pm,q_z}(\hat{b}_{\pm,q_z} + \hat{b}^\dagger_{\pm,-q_z}),
\end{aligned} \tag{C14}$$

where $\hat{\mathcal{V}}$ has experienced Landau quantization procedure, $|u_{s_z^\beta mk_z}\rangle$ is the periodic part of Bloch wave function $|\psi_{s_z^\beta mk_z}\rangle$, and $\hat{H}^{ep}$ is diagonal with respect to m index due to the selection rules. Similarly, for LA phonon we have

$$\begin{aligned}
\langle \psi_{s_z^\alpha mk_z}|\hat{\epsilon}_{zz}\hat{\mathcal{V}}_{zz}|\psi_{s_z^\beta m'k'_z}\rangle &= \frac{1}{\sqrt{N}} iq_z\xi_{zq_z}(\hat{b}_{zq_z} + \hat{b}^\dagger_{z,-q_z})\langle u_{s_z^\alpha mk_z+q_z}|\hat{\mathcal{V}}_{zz}|u_{s_z^\beta mk_z}\rangle\delta(k'_z+q_z-k_z)\delta(s_z^\alpha - s_z^\beta) \\
&\equiv \frac{1}{\sqrt{N}}\mathcal{G}_{mk_zz,q_z}(\hat{b}_{z,q_z} + \hat{b}^\dagger_{z,-q_z}).
\end{aligned} \tag{C15}$$

In realistic materials, it is not practical to calculate these integrals $\langle u_{s_z^\alpha mk_z+q_z}|\hat{\mathcal{V}}_{\lambda z}|u_{s_z^\beta mk_z}\rangle$ $(\lambda = \pm, z)$ either analytically or numerically. Thus, in the next section, we parametrize them based on the principles of symmetries.

2. Constrained by point group symmetries

In certain materials, electron-phonon coupling is constrained by the crystal symmetries. For Na_3Bi (no. 194 space group $P6_3/mmc$) at Γ point, the point group is

$6/mmm$ generated by rotations C_{3z}, C_{2z}, C_{110} and inversion P. For β-Ag_2Se (no. 19 space group $P2_12_12_1$) at Γ point, the point group is 222, generated by C_{2z} and C_{2x}. Here we consider three symmorphic symmetries of our interest: rotation, inversion, and mirror as their combination. Starting with the rotational symmetry, on the basis $\hat{\Psi}^\dagger_{mk_zQ} = (\hat{c}^\dagger_{\alpha mk_z+Q/2}, \hat{c}^\dagger_{\beta mk_z+Q/2}, \hat{c}^\dagger_{\alpha mk_z-Q/2}, \hat{c}^\dagger_{\beta mk_z-Q/2})^T$ (here we assume $s^\alpha_z > s^\beta_z$), up to the zeroth order of k_z, with the selection rule $\pm(s^\alpha_z - s^\beta_z) = l^{\mathrm{ph}}_{z,\mp,Q}$. And the angular momentum of chiral phonon is defined as

$$\begin{aligned}\hat{L}_{z,q_z} &= i\hbar(\hat{b}^\dagger_{x,q_z}\hat{b}_{y,q_z} - \hat{b}^\dagger_{y,q_z}\hat{b}_{x,q_z}) \\ &= \hbar(\hat{b}^\dagger_{-,q_z}\hat{b}_{-,q_z} - \hat{b}^\dagger_{+,q_z}\hat{b}_{+,q_z}),\end{aligned} \tag{C16}$$

where $\hat{b}^\dagger_{\pm,q_z} = (\hat{b}^\dagger_{x,q_z} \pm i\hat{b}^\dagger_{y,q_z})/\sqrt{2}$, $\hat{b}_{\pm,q_z} = (\hat{b}_{x,q_z} \mp i\hat{b}_{y,q_z})/\sqrt{2}$, and correspondingly $\hat{X}_{\pm,q_z} = (\hat{X}_{x,q_z} \pm i\hat{X}_{y,q_z})/\sqrt{2} = \xi_{\pm,q_z}(\hat{b}_{\mp,q_z} + \hat{b}^\dagger_{\pm,-q_z})$ given amplitudes $\xi_{x,q_z} = \xi_{y,q_z} = \xi_{\pm,q_z}$ due to the rotation symmetry.

Consider a certain phonon mode $\hat{u}_{\lambda q_z}(z,t) = \hat{X}_{\lambda q_z}(t)e^{iq_zz} + \hat{X}_{\lambda,-q_z}(t)e^{-iq_zz}$, the electron-phonon coupling Hamiltonian for the same n index Landau bands reads

$$\begin{aligned}\hat{\mathcal{H}}^{ep}_{mk_zq_z} &= \frac{1}{\sqrt{N}}\sum_\lambda [\tau_+\mathcal{G}_{mk_z\lambda q_z}\hat{X}_{\lambda q_z}/\xi_{\lambda q_z} + \mathrm{H.c.}]\hat{\Psi}^\dagger_{mk_zq_z}\hat{\Psi}_{mk_zq_z}, \\ \mathcal{G}_{mk_zz,q_z} &= iq_z\xi_{zq_z}(g_0\sigma_0 + g_z\sigma_z)\delta(s^\alpha_z - s^\beta_z), \\ \mathcal{G}_{mk_z\pm,q_z} &= iq_z\xi_{\pm q_z}g_\pm\sigma_\mp\delta(s^\alpha_z - s^\beta_z - l^{\mathrm{ph}}_{z,\pm}),\end{aligned} \tag{C17}$$

where the coupling coefficients are complex constants determined by specific materials. Note that, in the case of $|\boldsymbol{q}| = 0$, three acoustic normal modes correspond to global translations of the crystal, of which the displacement amplitude is not defined and such translations will not alter the electronic band structure. Therefore, it is assumed that these modes are skipped throughout this article. Considering that $g_0\sigma_0$ term means the coupling strengths between LA phonon and electrons while $g_z\sigma_z$ term controls the strength difference of coupling to two bands, either one is enough to introduce a CDW gap. Hence, we simply set $g_0 = 0$ in the numerical calculations to reduce complications.

To make the physical meaning of electron-phonon coupling clearer, we rewrite the above electron-phonon coupling $\mathcal{G}_{mk_z\lambda q_z}$ on the linearly polarized basis:

$$\begin{aligned}\sum_{\lambda=\pm}\mathcal{G}_{mk_z\lambda q_z}\hat{X}_{\lambda q_z}/\xi_{\lambda q_z} &= iq_z\begin{pmatrix} 0 & g_-(\hat{X}_{xq_z} - i\hat{X}_{yq_z}) \\ g_+(\hat{X}_{xq_z} + i\hat{X}_{yq_z}) & 0 \end{pmatrix} \\ &= iq_z\begin{pmatrix} 0 & (g_1 - ig_2)(\hat{X}_{xq_z} - i\hat{X}_{yq_z}) \\ (g_1 + ig_2)(\hat{X}_{xq_z} + i\hat{X}_{yq_z}) & 0 \end{pmatrix} \\ &\equiv iq_z(g_1\hat{\boldsymbol{X}}_{Tq_z}\cdot\boldsymbol{\sigma}_T + g_2\hat{\boldsymbol{X}}_{Tq_z}\times\boldsymbol{\sigma}_T),\end{aligned} \tag{C18}$$

where $g_1 = (g_- + g_+)/2$, $g_2 = i(g_- - g_+)/2$, $\hat{\boldsymbol{X}}_{Tq_z} = (\hat{X}_{xq_x}, \hat{X}_{yq_z})$, and $\boldsymbol{\sigma}_T = (\sigma_x, \sigma_y)$. These are exactly two possible forms of interactions between two vector operators: TA phonon normal coordinate and electron spin.

If inversion symmetry is considered, as in the Dirac semimetal case, electron-phonon coupling is supposed to be further constrained by $\mathcal{P}^{-1}\mathcal{G}_{\lambda k_zq_z}\mathcal{P} = \mathcal{G}^\dagger_{\lambda,-k_z,-q_z}$ with $\mathcal{P} = \sigma_z$, then $g_+ = -g^\star_-$. In Kramers-Weyl semimetal, a noncentrosymmetric system, this constraint is not enforced. Given additional mirror symmetry $\mathcal{M}_x = \mathcal{P}\mathcal{C}_{2x} = \sigma_y$, the $\hat{\boldsymbol{X}}_{Tq_z}\cdot\boldsymbol{\sigma}_T$ term is killed and we have

$$\sum_{\lambda=\pm}\mathcal{G}_{mk_z\lambda q_z}\hat{X}_{\lambda q_z}/\xi_{\lambda q_z} = iq_zg_2\hat{\boldsymbol{X}}_{Tq_z}\times\boldsymbol{\sigma}_T. \tag{C19}$$

APPENDIX D: EFFECTIVE MODELS IN QUANTUM LIMIT

1. Topological Dirac semimetal

Near the Γ point, on the basis $\hat{\Psi}^{D\dagger}_{\boldsymbol{k}} = (\hat{c}^\dagger_{1/2,\boldsymbol{k}}, \hat{c}^\dagger_{-1/2,\boldsymbol{k}}, \hat{c}^\dagger_{+3/2,\boldsymbol{k}}, \hat{c}^\dagger_{-3/2,\boldsymbol{k}})^T$, constrained by TRS $\mathcal{T} = \tau_0(i\sigma_y)\mathcal{K}$ with complex conjugation operator $\mathcal{K}$ and inversion symmetry $\mathcal{P} = \tau_z\sigma_0$, the effective Hamiltonian for Dirac semimetal Na_3Bi reads

$$\mathcal{H}^D_{\boldsymbol{k}} = \begin{pmatrix} m_{\boldsymbol{k}} & 0 & \hbar v_\perp k_+ & 0 \\ & m_{\boldsymbol{k}} & 0 & -\hbar v_\perp k_- \\ & & -m_{\boldsymbol{k}} & 0 \\ \dagger & & & -m_{\boldsymbol{k}} \end{pmatrix} - \mu, \tag{D1}$$

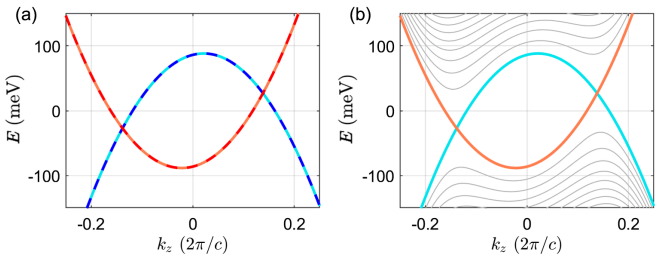

FIG. 4. (a) Band structures along k_z axis of Dirac semimetal when inversion symmetry is broken. (b) Landau bands when a strong magnetic field $B_z = 10$ T is applied.

where mass term $m_{\boldsymbol{k}} = m_\perp(k_x^2 + k_y^2) + m_z k_z^2 - m_0$. Let $\hat{a}^\dagger$ and $\hat{a}$ be Landau level creation and annihilation operators with $[\hat{a}, \hat{a}^\dagger] = 1$, the quantization scheme $k_x = (\hat{a} + \hat{a}^\dagger)/\sqrt{2}l_B$ and $k_y = i(\hat{a} - \hat{a}^\dagger)/\sqrt{2}l_B$ gives the magnetic Hamiltonian,

$$\hat{\mathcal{H}}^D_{k_z} = \begin{pmatrix} m_{k_z} & 0 & \frac{\sqrt{2}\hbar v_\perp}{l_B}\hat{a}^\dagger & 0 \\ & m_{k_z} & 0 & -\frac{\sqrt{2}\hbar v_\perp}{l_B}\hat{a} \\ & & -m_{k_z} & 0 \\ \dagger & & & -m_{k_z} \end{pmatrix} + \frac{2m_\perp}{l_B^2}\left(\hat{a}^\dagger\hat{a} + \frac{1}{2}\right)\tau_z\sigma_0 - \mu, \tag{D2}$$

on the Landau level basis $(|n\rangle, |n-1\rangle, |n-1\rangle, |n\rangle)^T$, where mass term becomes $m_{k_z} = m_z k_z^2 - m_0$. Then, the effective Hamiltonian for two lowest Landau bands on basis $(|0\rangle, |0\rangle)^T$ reads

$$\mathcal{H}^D_{0,k_z} = \left(m_{k_z} + \frac{m_\perp}{l_B^2}\right)\sigma_z - \mu\sigma_0, \tag{D3}$$

and all higher Landau bands ($n > 0$) are

$$E^D_{\pm n,k_z} = \pm\sqrt{\left(m_{k_z} + \frac{2m_\perp}{l_B^2}n\right)^2 + \frac{2\hbar^2 v_\perp^2}{l_B^2}n} \pm \frac{m_\perp}{l_B^2} - \mu. \tag{D4}$$

When $B_z = 10$ T, the "zero-point" energy $m_\perp/l_B^2$ is 0.0016 eV, much smaller than $m_0 = 0.086$ eV and negligible in the discussion of zeroth Landau bands.

As discussed in the main text, since two valleys are connected by inversion symmetry, two degenerate linearly polarized TA phonons will condensate simultaneously. However, if inversion symmetry is broken, two Dirac valleys are no longer degenerate, as shown in Fig. 4, and the ground state will be a self-twisting phase rather than a shear strain wave phase when TA phonons beat LA phonons.

2. Kramers-Weyl semimetal

On the basis $\hat{\Psi}^{\mathrm{KW}\dagger}_{\boldsymbol{k}} = (\hat{c}^\dagger_{1/2\boldsymbol{k}}, \hat{c}^\dagger_{-1/2\boldsymbol{k}})^T$, the effective Hamiltonian for Kramers-Weyl semimetal reads

$$\mathcal{H}^{\mathrm{KW}}_{\boldsymbol{k}} = (v_z k_z\sigma_z + v_\perp \boldsymbol{k}_\perp\cdot\boldsymbol{\sigma}_\perp) + (u_z k_z^2 + u_\perp \boldsymbol{k}_\perp^2 - \mu)\sigma_0. \tag{D5}$$

And its magnetic Hamiltonian will be

$$\hat{\mathcal{H}}^{\mathrm{KW}}_{k_z} = [v_z k_z\sigma_z + (u_z k_z^2 - \mu)\sigma_0] + u_\perp\frac{2}{l_B^2}\left(\hat{a}^\dagger\hat{a} + \frac{1}{2}\right)\sigma_0 + v_\perp\frac{\sqrt{2}}{l_B}(\hat{a}^\dagger\sigma_- + \hat{a}\sigma_+) + (-\delta_Z\sigma_z + \delta_T\sigma_x), \tag{D6}$$

where $\sigma_\pm = (\sigma_x \pm i\sigma_y)/2$, the first and second terms are directly from diagonal elements of the Hamiltonian, the third term is SOC, and the fourth term contains Zeeman effects $\delta_Z = g_z\mu_B B_z$ in z axis and rotation symmetry breaking term δ_T. Figure 5 is numerically computed on the Landau level basis $(|n\rangle, |n\rangle)^T$ with cutoff $n = 10$. To clearly show the influences of each term, we start with the band dispersion along the z axis shown in Fig. 2(a), then turn to the case with only Landau level effect of magnetic field considered. After that, the remaining terms are turned on one by one, to demonstrate the evolution of band structures shown in Fig. 5.

3. Mean-field approximation

In mean-field level, the phonon creation and annihilation operators are approximated by their expectation values leading to mean-field normal coordinates, then electron-phonon coupling of a certain phonon wave vector Q becomes

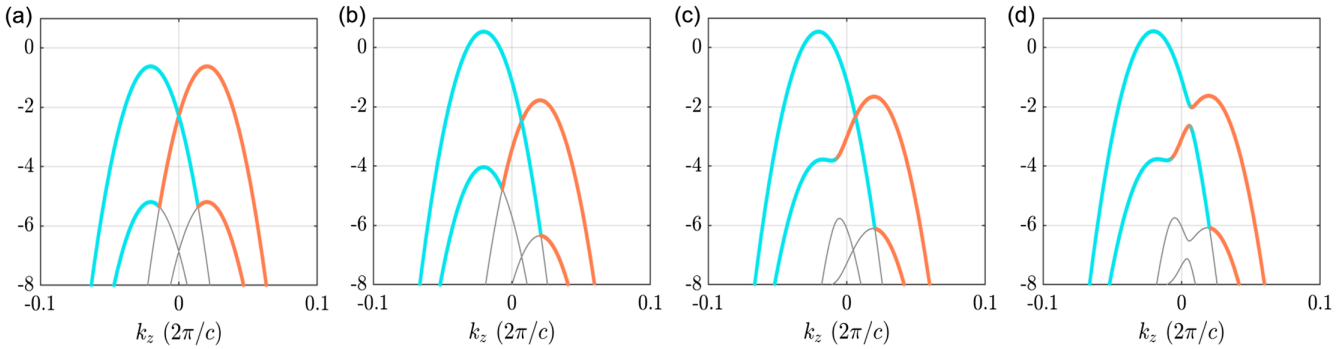

FIG. 5. Evolution of Landau bands of Kramers-Weyl semimetal. (a) Only Landau level effect, (b) Zeeman effect δ_Z added, (c) in-plane chiral coupling term (SOC) $v_\perp\boldsymbol{k}_\perp\cdot\boldsymbol{\sigma}_\perp$ considered, and (d) additional rotation symmetry breaking term δ_T.

$$\begin{aligned}
\hat{\tilde{H}}_Q^{ep} &= \frac{1}{N}\sum_{mk_z}\Delta_{mk_zQ}\hat{\Psi}^\dagger_{mk_zQ}\hat{\Psi}_{mk_zQ},\\
\Delta_{mk_zQ} &= \sum_\lambda \frac{1}{\sqrt{N}}\tau_+\mathcal{G}_{mk_z\lambda Q}(\langle\hat{b}_{\lambda Q}\rangle + \langle\hat{b}^\dagger_{\lambda,-Q}\rangle) + \text{H.c.}\\
&= \frac{1}{\sqrt{N}}\tau_+\begin{pmatrix} 0 & (1-ie^{i\phi_{xy}})\Delta_{-,Q}\\ (1+ie^{i\phi_{xy}})\Delta_{+,Q} & 0\end{pmatrix}\\
&\quad + \frac{1}{\sqrt{N}}\Delta_{z,Q}\tau_+\sigma_z + \text{H.c.},\\
\Delta_{\pm,Q} &= i2g_\pm Q\xi_{\pm,Q}\langle\hat{b}_{\pm,Q}\rangle e^{i\phi_x},\\
\Delta_{z,Q} &= i2g_{z0}Q\xi_{z,Q}\langle\hat{b}_{z,Q}\rangle e^{i\phi_z},
\end{aligned} \tag{D7}$$

where $\phi_{xy} = \phi_y - \phi_x$ is the relative phase between TA modes in x and y directions. In the centrosymmetric case, we have $g_+ = -g_-^\star$ and $\hat{\mathcal{P}}\hat{X}_{+,q_z}\hat{\mathcal{P}}^{-1} = \hat{X}^\dagger_{-,q_z}$, Meanwhile, $\Delta_{-,Q} = (\Delta_{+,Q})^\star$. By defining $\Delta_{T,Q} = |\Delta_{\pm,Q}|$, up to a unitary transformation, the order parameter from electron-TA phonon coupling is simplified to

$$\frac{1}{\sqrt{N}}\tau_+(\sigma_x + e^{i\phi_{xy}}\sigma_y)\Delta_{T,Q} + \text{H.c.} \tag{D8}$$

Thus, the total phonon energy is

$$\langle\hat{H}^{\text{ph}}_Q\rangle = \frac{1}{N}\sum_\lambda\hbar\omega_{\lambda Q}\langle\hat{b}^\dagger_{\lambda Q}\hat{b}_{\lambda Q}\rangle = \frac{1}{N}\sum_\lambda 2\hbar\omega_{\lambda Q}\langle\hat{b}_{\lambda Q}\rangle^2 = M\sum_\lambda(g_\lambda^{-1}v_\lambda^{\text{ph}}|\Delta_{\lambda Q}|)^2, \tag{D9}$$

where $\langle\hat{b}_{\mp,Q}\rangle = \langle\hat{b}^\dagger_{\pm,-Q}\rangle$ is assumed. Now we have the total electronic Hamiltonian with a certain phonon wave vector Q, in mean-field level,

$$\begin{aligned}
\bar{\mathcal{H}}^D_{k_zQ} &= (\mathcal{H}^D_{k_z+Q/2}\oplus\mathcal{H}^D_{k_z-Q/2} - \mu) + \tau_+[\Delta_{T,Q}(\sigma_x + e^{i\phi_{xy}}\sigma_y) + \Delta_{z,Q}\sigma_z] + \text{H.c.},\\
\mathcal{H}^D_{k_zQ} &= \begin{pmatrix} E_{-0,k_z} & 0\\ 0 & E_{+0,k_z}\end{pmatrix},
\end{aligned} \tag{D10}$$

for Dirac semimetal, and

$$\begin{aligned}
\bar{\mathcal{H}}^{\text{KW}}_{k_zQ} &= (\mathcal{H}^{\text{KW}}_{k_z+Q/2}\oplus\mathcal{H}^{\text{KW}}_{k_z-Q/2} - \mu) + \tau_+[\Delta_{T,Q}(1-e^{i\phi_{xy}})\sigma_+ + \Delta_{z,Q}\sigma_z] + \text{H.c.},\\
\mathcal{H}^{\text{KW}}_{k_zQ} &= \begin{pmatrix} E^{(1)}_{1/2,k_z} & \delta_T\\ \delta_T & E^{(1)}_{-1/2,k_z}\end{pmatrix},
\end{aligned} \tag{D11}$$

for Kramers-Weyl semiemtal with additional rotation symmetry breaking term δ_T.

APPENDIX E: RENORMALIZED PHONON DISPERSION

The Mastubara Green's function of "bare" phonon is

$$D^{(0)}_{\lambda\boldsymbol{q}}(i\nu_n) = \frac{2\omega_{\lambda\boldsymbol{q}}}{(i\nu_n)^2 - (\omega_{\lambda\boldsymbol{q}})^2}, \tag{E1}$$

where $\nu_n = 2\pi n/\beta$ is the Mastubara frequency. Consider electron-phonon coupling in random phase approximation and self-consistent Midgal approximation, the phonon Green function and phonon self-energy are

$$D^{-1}_{\lambda\boldsymbol{q}} = [D^{(0)}_{\lambda\boldsymbol{q}}]^{-1} - \Pi^{\text{ph}}_{\lambda q_z}, \qquad \Pi^{\text{ph}}_{\lambda q_z} = \frac{1}{\hbar}|\mathcal{G}_{\lambda\boldsymbol{q}}|^2\mathcal{L}_{\lambda\boldsymbol{q}}, \tag{E2}$$

where $\mathcal{L}_{\lambda\boldsymbol{q}}(\omega)$ is the Lindhard response function. The pole of $D_{\lambda\boldsymbol{q}}(i\nu_n)$ gives the renormalized phonon frequency $\omega^{\text{ren}}_{\lambda\boldsymbol{q}}$ in q_z direction,

$$\begin{aligned}
\Delta\omega^2_{\lambda q_z} &= (\omega^{\text{ren}}_{\lambda q_z})^2 - \omega^2_{\lambda q_z} = \frac{2}{\hbar}\omega_{\lambda q_z}|\mathcal{G}_{\lambda q_z}|^2\mathcal{L}_{\lambda q_z}(\omega^{\text{ren}}_{\lambda q_z})\\
&= \frac{(g_\lambda q_z)^2}{M}\mathcal{L}_{\lambda q_z}(\omega^{\text{ren}}_{\lambda q_z}),
\end{aligned} \tag{E3}$$

where the Lindhard response functions are

$$\begin{aligned}
\mathcal{L}_{\lambda q_z} &= \frac{1}{N_z}\sum_{\alpha\beta,k_z}\frac{\mathcal{S}_{\alpha\beta\lambda k_z q_z}(f_{\alpha k_z+q_z} - f_{\beta k_z})}{\varepsilon_{\alpha k_z+q_z} - \varepsilon_{\beta k_z} - \hbar(\omega + i\eta)},\\
\mathcal{S}_{\alpha\beta\lambda k_z q_z} &= \sum_{ij}\langle s^\beta_{z,k_z+q_z}|s^{(j)}_z\rangle\langle s^{(i)}_z|s^\alpha_{z,k_z}\rangle\delta(s^{(i)}_z - s^{(j)}_z - l^{\text{ph}}_{z,\lambda}),
\end{aligned} \tag{E4}$$

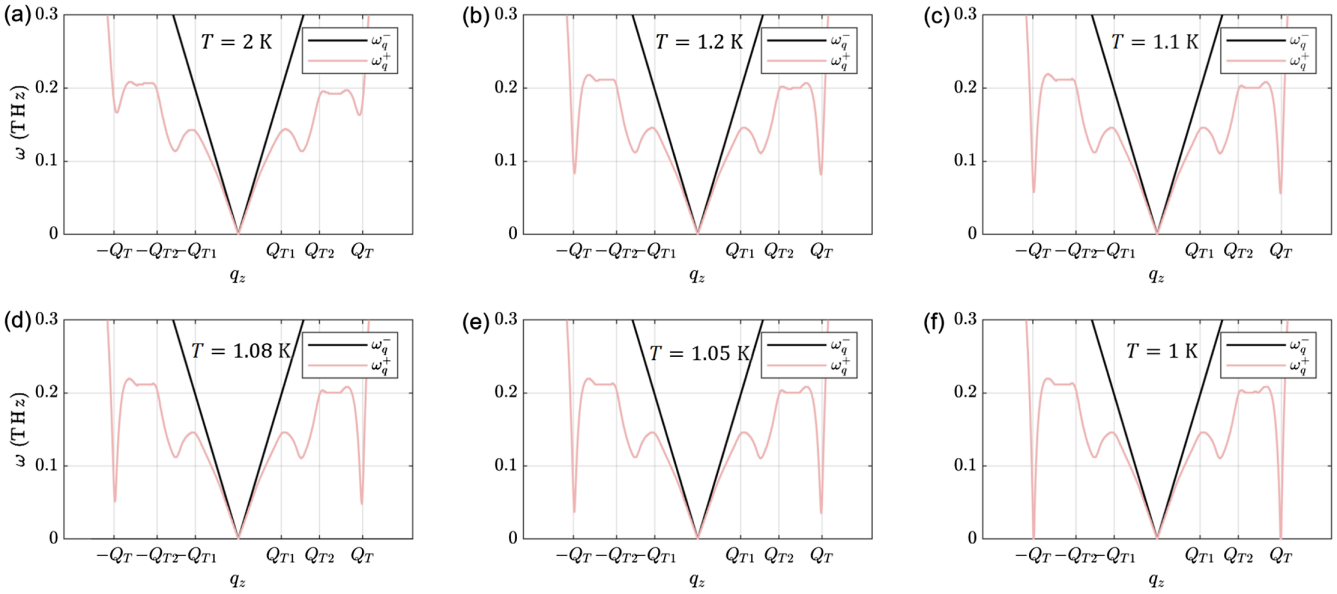

FIG. 6. Phonon frequencies of Kramers-Weyl semimetal under $B = 10$ T magnetic field at different temperatures.

where $f_{\alpha k_z} = 1/(e^{\varepsilon_{\alpha k_z}/k_B T} + 1)$ is the Fermi-Dirac distribution function, and i, j run over all possible spin components. When the electronic states are polarized to be independent on crystal momentum, $s^{\alpha}_{z,q_z} = s^{\alpha}_z$, $\mathcal{S}_{\alpha\beta\lambda k_z q_z}$ is reduced to the spin selection rule $\delta(s^{\alpha}_z - s^{\beta}_z - l^{\mathrm{ph}}_{z,\lambda})$.

For Na_3Bi and β-Ag_2Se, their bulk modulus (in the sense of Voigt-Reuss-Hill average) K is 17 and 58 GPa and their density ρ is 3.63 and 7.98 g/cm^3, respectively. By the definition of the Young's modulus $Y = 3K(1-2\sigma)$ and LA phonon group speed $v_s^L = \sqrt{Y/\rho}$, the LA wave speeds are estimated to be 2650 and 2088 m/s, respectively.

APPENDIX F: CHIRAL STANDING WAVE

At finite temperature, the dressed phonon frequencies from Eq. (E3) of a generic system have to be solved numerically. To get a flavor of the new standing modes with wave vector around $+Q_T$, we expand the Lindhard response function up to the first order of $\delta q_z^+ = q_z - Q_T$ and ω:

$$\mathcal{L}_{\lambda\delta q_z^+}(\omega) = \mathcal{L}_{\lambda}^{(0)} + \mathcal{L}_{\lambda}^{(1)}\delta q_z^+ + \mathcal{L}_{\lambda}^{(2)}\omega. \tag{F1}$$

Then Eq. (E3) becomes

$$\omega^2 - \frac{g_T^2}{M}(\mathcal{L}_{\lambda}^{(0)} + \mathcal{L}_{\lambda}^{(1)}\delta q_z^+ + \mathcal{L}_{\lambda}^{(2)}\omega)(\delta q_z^+ + Q_T)^2 - (v_T^{\mathrm{ph}})^2(\delta q_z^+ + Q_T)^2 = 0, \tag{F2}$$

where the nonzero $\mathcal{L}_{\lambda}^{(2)}$ is induced by TRS breaking, and we solve the effective frequency up to $(\delta q_z^+)^2$:

$$\omega_{\lambda\delta q_z^+}^{(+Q_T)} = \omega_{Q_T} + \frac{1}{2}b(\delta q_z^+)^2. \tag{F3}$$

As plotted in Fig. 6, the parabolic approximation is nearly valid within the $(0.95, 1.05)Q_T$ regime. Correspondingly, the discrete wave vectors for standing modes are $\delta q_n^+ = (n + N_s)\pi/d - Q_T \approx n\pi/d (n = 0, 1, \ldots)$, where N_s is a big positive number to cancel the finite Q_T. Thus, the frequency differences of these standing modes are

$$\omega_n^{(+Q_T)} = \omega_{Q_T} + \frac{1}{2}b(\delta q_n^+)^2. \tag{F4}$$

Around $-Q_T$, the dispersion could be different from the $+Q_T$ regime since time reversal, inversion, and rotation symmetries are broken. However, the Fermi surface can be simply treated as two points at low temperature, and the inversion symmetry is approximately recovered. Thus, the effective dispersion near $-Q_T$ in terms of $\delta q_n^- = (n - N)\pi/d - (-Q_T) \approx n\pi/d$ is

$$\omega_n^{(-Q_T)} = \omega_{Q_T} + \frac{1}{2}b(\delta q_n^-)^2. \tag{F5}$$

Given a resonant frequency $\omega > \omega_{Q_T}$, there are four degenerate left-handed traveling modes, $(\delta q_n^+, \omega_n^{(Q_T)})$, $(\delta q_{-n}^+, \omega_n^{(Q_T)})$, $(\delta q_n^-, \omega_n^{(-Q_T)})$, $(\delta q_{-n}^-, \omega_n^{(-Q_T)})$, existing to form two left-handed standing modes, and the frequency differences between two adjacent modes are

$$\Delta\omega_n^{(\pm Q_T)} = \omega_{n+1}^{(\pm Q_T)} - \omega_n^{(\pm Q_T)} = \frac{b\pi^2}{d^2}\left(n + \frac{1}{2}\right) \equiv \Delta\omega_n^{(Q_T)}. \tag{F6}$$

TABLE III. Resonant frequencies of standing modes at different temperatures.

Temperature (K)	b (m^2/s)	$\omega_n^{(0)}$ (kHz)	ω_{Q_T} (GHz)	$\Delta\omega_n^{(Q_T)}$ (kHz)
1.2	6.17×10^{-4}	$268n$	81.8	$0.061(n+1/2)$
1.1	8.71×10^{-4}	$268n$	56.1	$0.086(n+1/2)$
1.08	9.80×10^{-4}	$268n$	48.1	$0.097(n+1/2)$
1.05	12.0×10^{-4}	$268n$	35.3	$0.118(n+1/2)$

In the case of Ag_2Se when $T=1.1$ K, we have $Q_T=6.67\times10^8\ m^{-1}$, $\omega_Q=56.1$ GHz, and $b=8.71\times10^{-4}\ m^2/s$. The N_s in this case is 2.12×10^6. Given $d=1$ cm, we have $\omega_Q+\Delta\omega_n^{(Q)}=56.1\ \text{GHz}+0.086(n+1/2)\,\text{kHz}$. Meanwhile, we have another long wavelength standing wave, with $\omega_{n'}^{(0)}=nv_T^{\text{ph}}\pi/d=(268n')$ kHz. When n is small, the frequency difference between adjacent chiral standing modes is indistinguishable compared with long wavelength modes. However, $\Delta\omega_n^{(Q_T)}$ will be even larger than $\Delta\omega_{n'}^{(0)}$ after $n_c=3116$ and both of them should be measurable experimentally. As well, $n_c/N_s\approx0.15\%$ is a close neighbor of Q_T and the parabolic approximation of frequency dispersion still holds.

Because the effective dispersion is sensitive to temperature, we compute the phonon dispersions shown in Fig. 6, and the resonant frequencies at different temperatures are listed in Table III.

APPENDIX G: MAGNETOACOUSTIC BIREFRINGENCE

1. Faraday rotation

Since the right-handed and the left-handed TA acoustic waves propagate with different speeds, v_s^+ and v_s^-, in the gyromagnetic media, the linearly polarized wave becomes

$$\begin{aligned}\boldsymbol{X}(d,t)&=X_+e^{i(k_+d-\omega t)}\hat{e}_++X_-e^{i(k_-d-\omega t)}\hat{e}_-\\&=\frac{X}{2}[(e^{ik_+d}+e^{ik_-d})\hat{\boldsymbol{x}}+i(e^{ik_+d}-e^{ik_-d})\hat{\boldsymbol{y}}]e^{-i\omega t}\\&=Xe^{i[(k_++k_-)d/2-\omega t]}\\&\quad\times\left[\hat{\boldsymbol{x}}\cos\frac{(k_--k_+)d}{2}+\hat{\boldsymbol{y}}\sin\frac{(k_--k_+)d}{2}\right],\end{aligned}\tag{G1}$$

where $|X_\pm|=|X_x\pm iX_y|=X/\sqrt{2}$. The polarization plane therefore rotates by a Faraday angle,

$$\begin{aligned}\theta_F&=\left|\tan^{-1}\frac{X_y}{X_x}\right|=\frac{d}{2}|k_--k_+|=\frac{d}{2}\left|\frac{\omega}{v_-^{\text{ph}}}-\frac{\omega}{v_+^{\text{ph}}}\right|\\&=\frac{\omega d}{2v_T^{\text{ph}}}\left(1-\frac{v_T^{\text{ph}}}{v_+^{\text{ph}}}\right)\equiv\mathcal{V}B_zd,\end{aligned}\tag{G2}$$

where we used the left-handed TA wave speed $v_-^{\text{ph}}=v_T^{\text{ph}}$, and $\mathcal{V}$ denotes the Verdet coefficient, which is in general a nonlinear function depending on frequency rather than a constant. Then it is numerically estimated that $v_+^{\text{ph}}=1811$ m/s (another possibility -1811 m/s is dropped) for the $\omega=58.0$ GHz acoustic waves when $T=1.1$ K, $|g_T/g_{z0}|=1.43\times10^{-4}$, $B_z=10$ T, and $\delta_T=1.2$ meV for Kramers-Weyl semimetal β-Ag_2Se system. Consider that $v_T^{\text{ph}}=v_z^{\text{ph}}\sqrt{(1+\sigma)/(2-2\sigma)}=852$ m/s, we find a giant Faraday rotation with $\theta_F/d=1.77\times10^5$ rad/cm.

2. Kerr ellipticity in polar configuration

In optics, according to the relative configuration of incident light and magnetic materials, there are three types of magneto-optical Kerr effects: polar, longitudinal, and transverse. Similarly, we also have three configurations in the acoustical counterpart. For simplicity, here we only take the polar configuration near normal incidence as an example since it has larger effect than the other two. The reflection coefficients for two chiral acoustic waves are obtained through Fresnel relations:

$$r_+=\left|\frac{1-n_+/n_T}{1+n_+/n_T}\right|=0.262,\quad r_-=\left|\frac{1-n_-/n^T}{1+n_-/n_T}\right|=0.109,\tag{G3}$$

where we used $n^-/n^T=v_T^{\text{ph,CPVC}}/v_T^{\text{ph,KW}}=1060/852=1.244$ and $n^+/n^T=v_s^{\text{ph,CPVC}}/v_+^{\text{ph,KW}}=1060/1811=0.585$. The left-handed TA wave will be completely incident into the gyromagnetic material, while a proportion of the right-hand rotating wave can reflect with nonzero reflection coefficient r_+. So the Kerr ellipticity $\epsilon^K=(r_+-r_-)/(r_++r_-)=0.412$.

APPENDIX H: FIRST-PRINCIPLES CACULATIONS OF Na_3Bi

All calculations were performed using density-functional theory (DFT) and density-functional perturbation theory, pseudopotentials, and plane waves basis sets as implemented in the QUANTUM EXPRESSO suite [37,38]. We employed the Perdew–Burke–Ernzerhof exchange-correlation functional [39], optimized norm-conserving pseudopotentials [40] from the PSEUDO-DOJO library [41] for total energy and lattice dynamics calculations, and the plane

TABLE IV. Lattice constants and atomic parameters of Na_3Bi.

Space group	$P6_3/mmc$	Atom (Wyckoff position)	x	y	z
a (Å)	5.448	Na1 ($2b$)	0	0	1/4
b (Å)	5.448	Na2 ($4f$)	1/3	2/3	0.583
c (Å)	9.655	Bi ($2c$)	1/3	2/3	1/4

waves kinetic energy cutoffs are set to achieve 1 meV accuracy as recommended in these libraries. The convergence criterion for the ionic steps was that the forces on every ion were less than 0.01 eV/Å.

The crystallographic data for Na_3Bi are listed in Table IV [16,42]. We used a Γ-centered $8 \times 8 \times 4$ k-point grid. Two well-known Dirac points near the Fermi level lie at the Γ-A axis, as shown in Figs. 7(b) and 7(c). The phonon calculation employs a Γ-centered $4 \times 4 \times 2$ q-point grid and its convergence threshold needs to be refined to 10^{-16} (in atomic unit) to achieve convergence after many tests. Along the Γ-A direction, all acoustic phonon modes are almost linear and two TA phonon modes are degenerate as shown in Fig. 7(d), which well satisfies our assumption for the speeds of acoustic phonons in the main text. The phonon self-energy based on electron-phonon coupling g matrix is computed by using the software package EPW [43]. In Fig. 7(e), we plot the coupling strength between valance and conductance bands with TA and LA phonon modes at two specific phonon wave vectors: long wavelength limit $Q = 0.06$ and finite wave vector $Q = 0.31$ connecting two Dirac cones. First, the magnitude of $|g|$ is around 0.2–1.0 eV, which justifies our parameter 0.5 eV used in the model. Along the Γ-A direction, the speed of TA phonon v_T^{ph} is around half of a LA phonon v_L^{ph}, as shown in Fig. 7(d). According to our analysis of Na_3Bi in the main text, the shear strain wave is favored when $|g_T^D/g_L^D| > v_T^{\mathrm{ph}}/v_L^{\mathrm{ph}} \approx 0.5$. And the electron-TA phonon coupling strength $|g_T^D|$ is similar and even stronger than electron-LA phonon coupling $|g_L^D|$. Therefore, it is promising to predict that shear strain wave phase could be the ground state of Na_3Bi at zero temperature.

APPENDIX I: ESTIMATION OF CORRECTION TO EINSTEIN–DE HASS EFFECT

With external magnetic field $B = 5$ T, the rotation symmetry breaking term $\delta_T = 0.2$ meV, the renormalized phonon dispersion, and density of state (DOS) of each chiral acoustic phonon mode are as shown in Fig. 8(b).

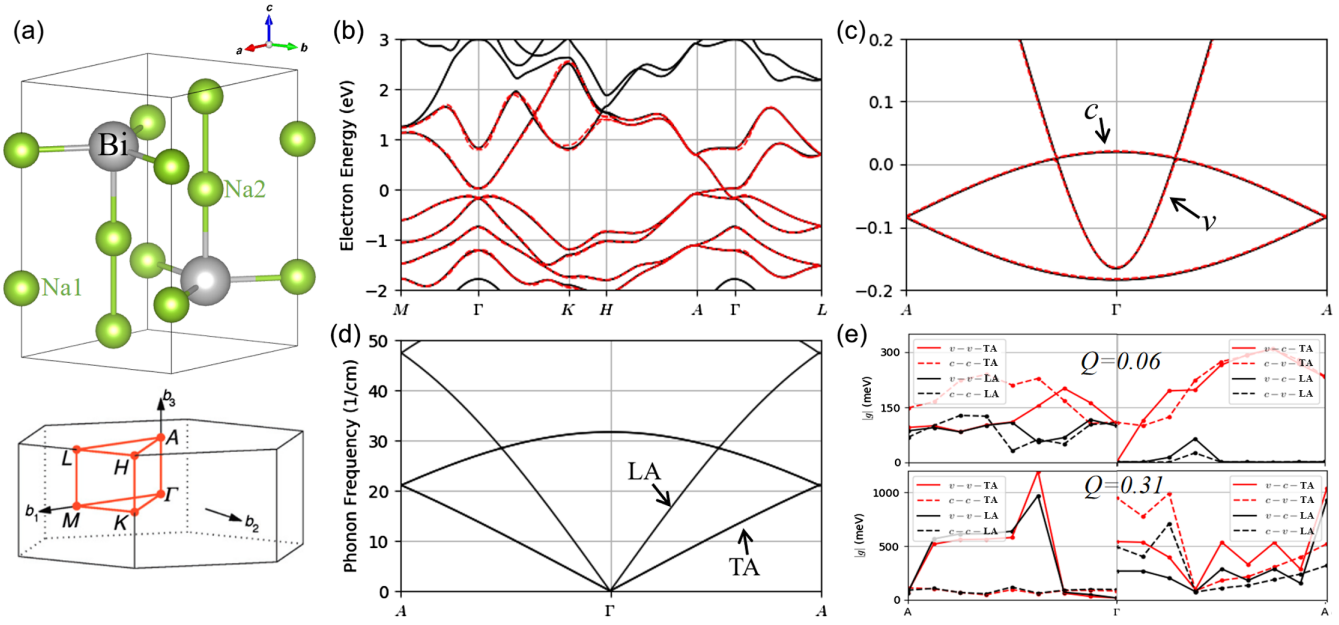

FIG. 7. (a) Upper: crystal structure of Na_3Bi. Two Na1 atoms (green), four Na2 atoms (green), and two Bi atoms (gray) lie at $2b$, $4f$, and $2c$ Wyckoff positions, respectively. Bottom: Brillouin zone (BZ) and high-symmetry path used in the electron and phonon calculations. (b) Band structures (black lines) from DFT of Na_3Bi with SOC included. Twelve low-energy bands (red lines) based on maximally localized Wannier functions using the prior selected columns of the density matrix (SCDM) method. (c) Enlarged view of band structure near Γ point. c and v refer to the conduction and valence bands near Fermi level. (d) Acoustic phonon dispersion in the Z-Γ-Z path with rotation symmetry. Longitudinal acoustic (LA) and degenerate transverse acoustic (TA) phonon branches are almost linear until the BZ boundary. (e) $|g|$-matrix elements of TA and LA phonon modes coupling to the c and v bands. Upper: in the long wavelength limit where we select a $Q = 0.06$ (in unit of reciprocal lattice constant) example, the left is the intraband coupling and the right is the interband coupling. Red (balck) lines refer to TA (LA) phonon modes and solid (dashed) lines refer to valance (conductance) band. Bottom: in the finite wave vector case where we select a $Q = 0.31$ (the wave vector connecting two Dirac cones) phonon mode. Color and line type follow the same convention as the upper figure.

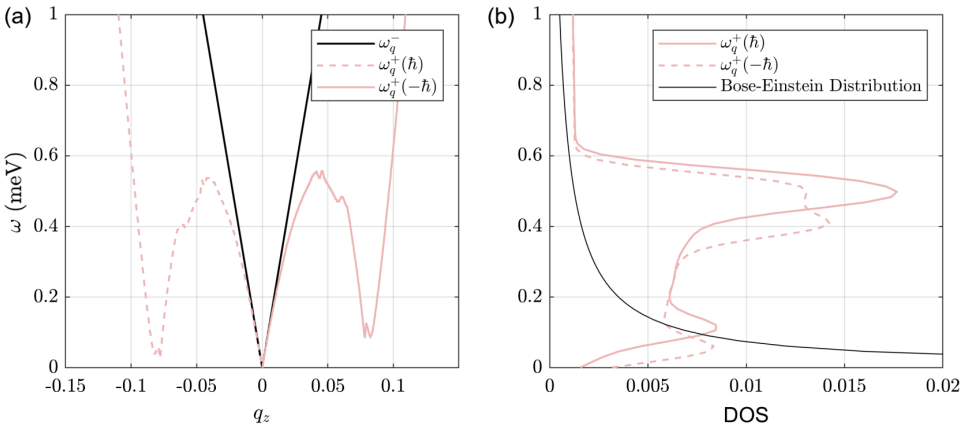

FIG. 8. (a) Renormalized phonon dispersion of β-Ag_2Se at temperature $T = 15.7$ K, where the applied magnetic field is $B = 5$ T and the rotation symmetry breaking term is $\delta_T = 0.2$ meV. (b) Corresponding density of states (DOS) of each chiral phonon mode. Solid (dashed) red line refers to phonon mode with $+\hbar$ $(-\hbar)$ angular momentum. The black line is the Bose-Einstein distribution at $T = 15.7$ K. The DOS of unscreened phonon modes $(\omega_q^{(-)})$ are not plotted because their angular momenta are exactly canceled out.

Inherited from sensitivity of phonon dispersion to temperatures, the net phonon angular momentum is also quite sensitive. At three different temperatures, 15.65, 15.7, and 15.8 K, the net phonon angular momentum per unit cell is $-2.7 \times 10^{-3}\hbar$, $-1.5 \times 10^{-3}\hbar$, and $-1.47 \times 10^{-4}\hbar$, respectively. They are close, in the order of magnitude, to the estimation of paramagnetic materials CeF_3 and $Tb_3Ga_5O_{12}$ in the literature [36].

[1] G. Grüner, *The Dynamics of Charge-Density Waves*, Rev. Mod. Phys. **60**, 1129 (1988).
[2] Grüner, *Density Waves in Solids* (CRC Press, Boca Raton, FL, 1994).
[3] G. Grimvall, *The Electron-Phonon Interaction in Metals* (North-Holland, Amsterdam, 1981).
[4] F. Giustino, *Electron-Phonon Interactions from First Principles*, Rev. Mod. Phys. **89**, 015003 (2017).
[5] N. P. Armitage, E. J. Mele, and A. Vishwanath, *Weyl and Dirac Semimetals in Three-Dimensional Solids*, Rev. Mod. Phys. **90**, 015001 (2018).
[6] B. I. Halperin, *Possible States for a Three-Dimensional Electron Gas in a Strong Magnetic Field*, Jpn. J. Appl. Phys. **26**, 1913 (1987).
[7] M. Kohmoto, B. I. Halperin, and Y.-S. Wu, *Diophantine Equation for the Three-Dimensional Quantum Hall Effect*, Phys. Rev. B **45**, 13488 (1992).
[8] H. L. Störmer, J. P. Eisenstein, A. C. Gossard, W. Wiegmann, and K. Baldwin, *Quantization of the Hall Effect in an Anisotropic Three-Dimensional Electronic System*, Phys. Rev. Lett. **56**, 85 (1986).
[9] F. Tang, Y. Ren, P. Wang, R. Zhong, J. Schneeloch, S. A. Yang, K. Yang, P. A. Lee, G. Gu, Z. Qiao *et al.*, *Three-Dimensional Quantum Hall Effect and Metal–Insulator Transition in* $ZrTe_5$, Nature (London) **569**, 537 (2019).
[10] F. Qin, S. Li, Z. Z. Du, C. M. Wang, W. Zhang, D. Yu, H.-Z. Lu, and X. C. Xie, *Theory for the Charge-Density-Wave Mechanism of 3D Quantum Hall Effect*, Phys. Rev. Lett. **125**, 206601 (2020).
[11] Z. F. Ezawa, *Quantum Hall Effects: Field Theoretical Approach and Related Topics* (World Scientific Publishing Company, Singapore, 2008).
[12] G. L. Bir and G. E. Pikus, *Symmetry and Strain-Induced Effects in Semiconductors* (Wiley, New York, 1974), Vol. 624.
[13] W. P. Dumke, *Deformation Potential Theory for n-Type Ge*, Phys. Rev. **101**, 531 (1956).
[14] G. D. Mahan, *Many-Particle Physics*, 3rd ed. (Kluwer Academic/Plenum Publishers, New York, 2013).
[15] Z. Wang, H. Weng, Q. Wu, X. Dai, and Z. Fang, *Three-Dimensional Dirac Semimetal and Quantum Transport in* Cd_3As_2, Phys. Rev. B **88**, 125427 (2013).
[16] Z. Wang, Y. Sun, X.-Q. Chen, C. Franchini, G. Xu, H. Weng, X. Dai, and Z. Fang, *Dirac Semimetal and Topological Phase Transitions in* A_3Bi *(*$A = Na, K, Rb$*)*, Phys. Rev. B **85**, 195320 (2012).
[17] Z. Liu, B. Zhou, Y. Zhang, Z. Wang, H. Weng, D. Prabhakaran, S.-K. Mo, Z. Shen, Z. Fang, X. Dai *et al.*, *Discovery of a Three-Dimensional Topological Dirac Semimetal,* Na_3Bi, Science **343**, 864 (2014).
[18] Z. Liu, J. Jiang, B. Zhou, Z. Wang, Y. Zhang, H. Weng, D. Prabhakaran, S. K. Mo, H. Peng, P. Dudin *et al.*, *A Stable Three-Dimensional Topological Dirac Semimetal* Cd_3As_2, Nat. Mater. **13**, 677 (2014).
[19] B. Wan, F. Schindler, K. Wang, K. Wu, X. Wan, T. Neupert, and H.-Z. Lu, *Theory for the Negative Longitudinal Magnetoresistance in the Quantum Limit of Kramers Weyl Semimetals*, J. Phys. Condens. Matter **30**, 505501 (2018).
[20] P. Li, B. Lv, Y. Fang, W. Guo, Z. Wu, Y. Wu, D. Shen, Y. Nie, L. Petaccia, C. Cao *et al.*, *Charge Density Wave and Weak Kondo Effect in a Dirac Semimetal CeSbTe*, Sci. China Phys. Mech. Astron. **64**, 237412 (2021).
[21] W. Shi, B. J. Wieder, H. L. Meyerheim, Y. Sun, Y. Zhang, Y. Li, L. Shen, Y. Qi, L. Yang, J. Jena *et al.*, *A Charge-Density-Wave Topological Semimetal*, Nat. Phys. **17**, 381 (2021).

[22] C.-L. Zhang, F. Schindler, H. Liu, T.-R. Chang, S.-Y. Xu, G. Chang, W. Hua, H. Jiang, Z. Yuan, J. Sun *et al.*, *Ultraquantum Magnetoresistance in the Kramers-Weyl Semimetal Candidate β-Ag_2Se*, Phys. Rev. B **96**, 165148 (2017).

[23] G. Chang, B. J. Wieder, F. Schindler, D. S. Sanchez, I. Belopolski, S.-M. Huang, B. Singh, D. Wu, T.-R. Chang, T. Neupert *et al.*, *Topological Quantum Properties of Chiral Crystals*, Nat. Mater. **17**, 978 (2018).

[24] H. Chen, W. Wu, J. Zhu, Z. Yang, W. Gong, W. Gao, S. A. Yang, and L. Zhang, *Chiral Phonon Diode Effect in Chiral Crystals*, Nano Lett. **22**, 1688 (2022).

[25] T. Zhang and S. Murakami, *Chiral Phonons and Pseudoangular Momentum in Nonsymmorphic Systems*, Phys. Rev. Res. **4**, L012024 (2022).

[26] T. Zhang and S. Murakami, *Chiral Phonons Entangled with Multiple Hall Effects and Unified Convention for Pseudoangular Momentum in Two-Dimensional Materials*, Phys. Rev. B **105**, 235204 (2022).

[27] D. L. Portigal and E. Burstein, *Acoustical Activity and Other First-Order Spatial Dispersion Effects in Crystals*, Phys. Rev. **170**, 673 (1968).

[28] T. Frenzel, J. Köpfler, E. Jung, M. Kadic, and M. Wegener, *Ultrasound Experiments on Acoustical Activity in Chiral Mechanical Metamaterials*, Nat. Commun. **10**, 3384 (2019).

[29] B. Lüthi, *Physical Acoustics in the Solid State* (Springer Berlin, Heidelberg, 2005).

[30] A. K. Zvezdin and V. A. Kotov, *Modern Magnetooptics and Magnetooptical Materials* (CRC Press, Boca Raton, FL, 1997).

[31] A. Pine, *Direct Observation of Acoustical Activity in α Quartz*, Phys. Rev. B **2**, 2049 (1970).

[32] J. Joffrin and A. Levelut, *Mise en Evidence et Mesure du Pouvoir Rotatoire Acoustique Naturel du Quartz-α*, Solid State Commun. **8**, 1573 (1970).

[33] Y. Lee, T. Haard, W. P. Halperin, and J. A. Sauls, *Discovery of the Acoustic Faraday Effect in Superfluid 3 he-b*, Nature (London) **400**, 431 (1999).

[34] J. Sauls, Y. Lee, T. Haard, and W. Halperin, *Magneto-acoustic rotation of transverse waves in* ^{3}He-B, Physica (Amsterdam) **284B**, 267 (2000).

[35] A. Einstein and W. J. de Haas, *Experimenteller Nachweis der Ampereschen Molekularströme*, Verh. Dtsch. Phys. Ges. **17**, 152 (1915).

[36] L. Zhang and Q. Niu, *Angular Momentum of Phonons and the Einstein—de Haas Effect*, Phys. Rev. Lett. **112**, 085503 (2014).

[37] P. Giannozzi, S. Baroni, N. Bonini, M. Calandra, R. Car, C. Cavazzoni, D. Ceresoli, G. L. Chiarotti, M. Cococcioni, I. Dabo *et al.*, *QUANTUM ESPRESSO: A Modular and Open-Source Software Project for Quantum Simulations of Materials*, J. Phys. Condens. Matter **21**, 395502 (2009).

[38] P. Giannozzi, O. Andreussi, T. Brumme, O. Bunau, M. B. Nardelli, M. Calandra, R. Car, C. Cavazzoni, D. Ceresoli, M. Cococcioni *et al.*, *Advanced Capabilities for Materials Modelling with QUANTUM ESPRESSO*, J. Phys. Condens. Matter **29**, 465901 (2017).

[39] J. P. Perdew, K. Burke, and M. Ernzerhof, *Generalized Gradient Approximation Made Simple*, Phys. Rev. Lett. **77**, 3865 (1996).

[40] D. R. Hamann, *Optimized Norm-Conserving Vanderbilt Pseudopotentials*, Phys. Rev. B **88**, 085117 (2013).

[41] M. J. van Setten, M. Giantomassi, E. Bousquet, M. J. Verstraete, D. R. Hamann, X. Gonze, and G.-M. Rignanese, *The PseudoDojo: Training and Grading a 85 Element Optimized Norm-Conserving Pseudopotential Table*, Comput. Phys. Commun. **226**, 39 (2018).

[42] G. Brauer and E. Zintl, *Konstitution von Phosphiden, Arseniden, Antimoniden und Wismutiden des Lithiums, Natriums und Kaliums*, Z. Phys. Chem., Abt. B **37**, 323 (1937).

[43] S. Poncé, E. R. Margine, C. Verdi, and F. Giustino, *EPW: Electron–Phonon Coupling, Transport and Superconducting Properties Using Maximally Localized Wannier Functions*, Comput. Phys. Commun. **209**, 116 (2016).